# FAB APPLICATION

*Une application de la méthode FAB à une base des données des surcotes de pleine mer, c'est à dire la partie considérée comme aléatoire du niveau marin, est développée dans ce chapitre.*

*La base de données est constituée par des sériés temporelles de surcotes de pleine mer systématiques provenant de 74 ports situés dans l'Atlantique, dans la Manche, dans la Mer d'Irlande et dans la Mer du Nord, et par 14 surcotes de pleine mer historiques.*

*La première étape de la FAB méthode consiste à former des régions physiques par la méthode de clustering des tempêtes définie dans l'approche AFR. Cette méthode de clustering est fondée sur la définition de trois paramètres physiques ($p$, $\Delta$, $\eta$). Pour des séries temporelles avec une différente durée, une analyse de sensibilité de ces paramètres est conseillée. La formation des régions physiques est recommandée pour une fenêtre temporelle dans laquelle la plupart des marégraphes sont en fonction.*

*Les autres étapes de la méthode FAB sont réalisées exclusivement pour les régions comprenant des sites avec des données historiques disponibles (Région 1 et Région 2). Les seuils optimaux sont évalués pour ces deux régions qui sont ensuite statistiquement vérifiées. Des niveaux de retour fréquentistes et bayésiens sont estimés et une comparaison préliminaire des résultats est montrée. Enfin, la méthode FAB est appliquée sur la même base de données sans surcotes historiques. Cette analyse supplémentaire permet d'indiquer le rôle des données historiques dans l'analyse régionale des événements extrêmes.*

# 4.1 Introduction

FAB method is applied to a database of systematic and historical skew surges illustrated in the following. This application permits the practical steps of the FAB methodology. Starting from a database of systematic and historical variables, this method enables the estimations of regional and local return levels.

After the collection of systematic and historical data from different locations, FAB method requires to pool sites in homogeneous regions in order to form regional samples and to treat them with a statistical analysis. In particular, physical homogeneous regions are formed through the definition of three parameters $p$, $\Delta$ and $\eta$. These parameters leading the formation of storm clusters have to be calibrated for time series with different periods of observation. For this reason, a sensitivity analysis of these three parameters is performed in this application. This sensitivity analysis is recommended when the FAB method is applied to a database of time series with different recording periods. Moreover, it is important to recall that in the FAB application case of the paper illustrated in Annexe A, the three parameters to form physical homogeneous regions were not calibrated. In that case, the parameters used were the same proposed in the RFA approach.

Now, physical homogeneous regions can be statistically verified. A double threshold approach is used and so a statistical threshold has to be defined in every site of the region. The statistical threshold chosen corresponds to a number of storms $\lambda$ per year above this threshold. This $\lambda$ value is common for every site in the region. The optimal value of $\lambda_{opt,r}$ has to be found for each physical region $r$ in order to get the best performances of this methodology on the extreme estimations. The identification of the $\lambda_{opt,r}$ based on a weighting analysis of sensitivity indicators is performed for the skew surge database.

The regional extreme data sample is then formed and the degree of dependence as the local and regional credible durations are computed. The GPD distribution is estimated for the sample of regional storms considering the seasonality of skew surges in the frequentist framework. No seasonality on skew surges is considered in the estimations of Bayesian return levels. Frequentist and Bayesian regional return levels and frequentist and Bayesian local return levels of each site by the use of the local indexes are estimated. This can allow the comparison between frequentist and Bayesian estimations always recalling the different concept of probabilities that the two statistical inferences have (Annexe B).

In such way, FAB method is applied to a database of 74 skew surge time series composed by systematic and historical data. In particular, the process of formation of physical and statistical regions states that sites in which historical skew surges are available belong to the Region 1 and the Region 2. For this reason, the FAB method is only focused on the frequentist and Bayesian estimations of return levels of these two regions.

# 4.2 Skew surge database

In this application, the maritime variable analysed is the skew surge. A skew surge database composed of systematic and historical skew surges is used to perform the FAB method.

Systematic skew surges are generated from time series recorded by tide gauges in different sites located along the coasts of Atlantic Ocean, the North Sea and the English Channel. Conversely, historical skew surges are collected in some French sites of Atlantic Ocean and the English Channel.

For this reason, the database of skew surges used in this application is formed by a systematic skew surge database in which historical skew surges are successively added.

## 4.2.1 Definition of skew surge

The sea level can be schematically shown as the overlap of two contributions: the predicted astronomical tide (deterministic part of sea level) and the instantaneous surge or residual (stochastic part of water level provoked by the meteorological variables).

As Fig. 8 shown, skew surge is defined as the difference between the maximum water level measured by a tide gauge and the maximum predicted astronomical tide computed during the same tidal cycle (Simon, 2007; Kerdagallan, 2013; Weiss, 2014).

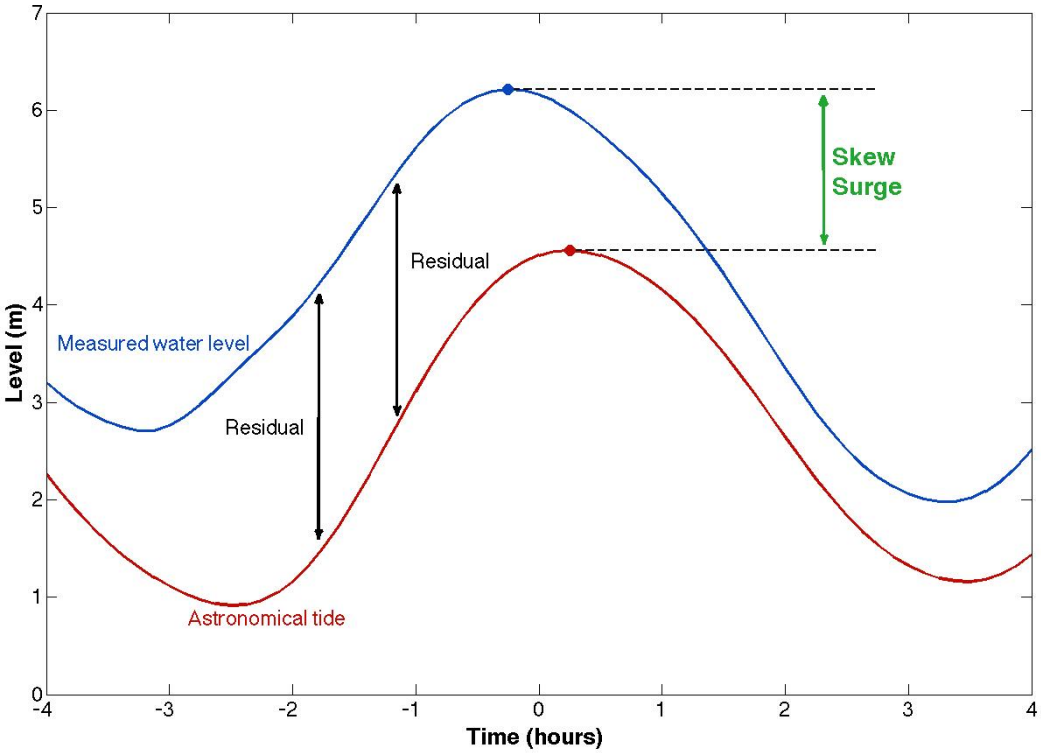


*Fig. 8 – Definition of skew surge. Source: SurgeWatch Glossary (University Southampton)*

Skew surges are preferred to instantaneous surges when dealing with extreme sea level. In fact, notwithstanding it is complicate get accurate and continuous time series of instantaneous surges, they are not influenced by a possible time lag between astronomical tides and sea levels. In addition, astronomical tides and residuals can have a possible dependence in the instant of maximum sea level and this has to be considerate in the computation of extreme sea levels (Weiss, 2014).

Finally, the knowledge of predicted astronomical tides and sea levels enables the calculation of time series of systematic skew surges and historical skew surge values.

### 4.2.2 Systematic skew surge database

The database of systematic skew surges is generated through sea levels data recorded by tide gauges. The quality of these water level measurements is checked by different national ocean data centers that provided these data. A big effort has been done during the acquisition of tidal gauge measurements in order to create a database of systematic skew surges as biggest as possible.

In addition, astronomical tides or residuals must be available to compute time series of systematic skew surges.

Data recorded by 74 tidal gauges located in French, Spanish, British and Belgian coasts of Atlantic Ocean, English Channel, Irish Sea and North Sea are considered in this study. The location of the 74 sites in which measurements of water levels are available is shown in Fig. 9. Time series of skew surges are successively computed for each of the 74 sites.

Sea level measurements of the 23 tidal gauges placed in French coasts are provided by the SHOM (Service Hydrographique et Océanographique de la Marine) and REFMAR (Réseaux de référence des observations marégraphiques) every hour. Time series of skew surges for French sites are created by the astronomical tides generated through the official software PREDIT provided by the SHOM.

Sea level measurements of 46 tidal gauges placed in British coasts are provided by the BODC (British Oceanographic Data Center) every hour until 1992 and every 15 minutes after 1993. In addition, the BODC supplies also residuals. This allows the computation of astronomical tides and consequently of the skew surges for each tidal cycle.

Only 2 Spanish sites in which water levels are provided by IEO (Instituto Español de Oceanografía) every hour are considered. Skew surges are calculated for the 2 Spanish sites by astronomical tides computed through the software SHOMAR (provided by the SHOM).

MVB (Meetnet Vlaamse Banken) has kindly provided the water levels for 3 Belgian sites (Nieuwpoort, Oostende et Zeebrugge) and the astronomical tides associated every 5 minutes. Skew surges are then calculated for these 3 Belgian ports.


*Fig. 9 - Location of 74 tide gauges considered in this study. Source of the map: Google Maps.*

This database can be considered as an update of the skew surge database used by Weiss (2014) for the application of the RFA approach. In particular, French and British data are available until 2017, data from sites like Dielette (France), Port Ellen (UK), Portbury (UK) and Bournemouth (UK) are exploitable, Belgian tide gauge measurements are considered and an important restoration of the time series at Saint-Nazaire had been done by the SHOM (Ferret, 2016) and these data are now available since 1821 (this time series' reconstruction has been used in this study even though the SHOM had recently retired these data to definitively validate them).

Before the computation of systematic skew surges for all sites, the sea levels measured in each site must be corrected by a likely significant eustatism. The eustatism is the modification of mean sea level caused mainly by ocean floor motion and ice sheet melting. Not ever the eustatism gives a remarkable contribution in sea levels and so not ever it has to be taken into account in sea level corrections. Eustatism is considered significant when the regression curve slop of

annual mean of sea levels can be practically considered void (p-value of T-Student test lower than 5% (Watson, 2016)). The eustatism for 67 of 74 sites was already calculated by Weiss (2014) until the year 2010. In cases in which eustatism is considered as significant, sea levels (recorded before 2010) are corrected by the same eustatism computed by Weiss (2014) apart from the site of Saint-Nazaire in which the eustatism has been entirely recalculated. For sea levels between 2011 and 2017, eustatism is considered irrelevant (only 6-7 years more of water level measurements).

Sea levels recorded by tide gauge at Saint-Nazaire has been corrected by an eustatism of 1,76 mm/year until the year 1893. Before this period, the regression curve slop is broken and not more tendency on sea levels are detected. For the 7 additional sites used in this study (3 British sites, 3 Belgian sites and 1 French site), no eustatism is detected and sea levels have no need to be corrected.

Every site has its own period of tidal recordings that depends on many factors. For instance, this could depend on the time in which tidal gauge is put into operation or damage on measurements during a big storm. The longest period of sea levels measurements is available for the tide gauge located at Brest: 156.57 years of recordings since 1846 (Fig. 10).

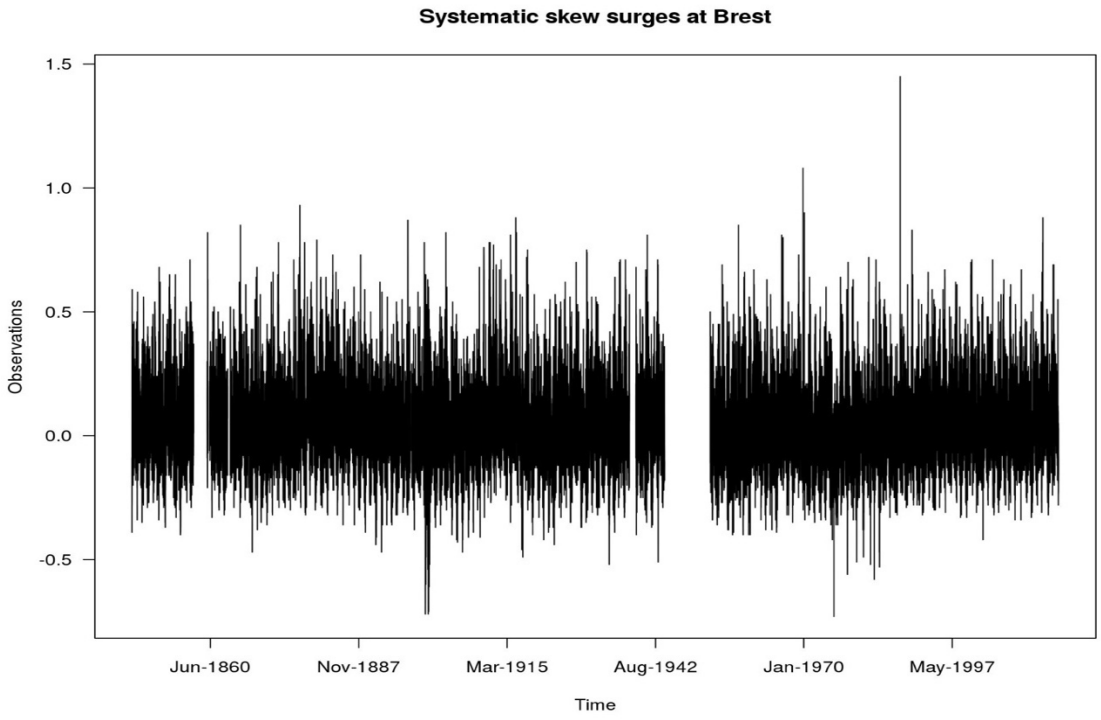


*Fig. 10 - The longest time series of skew surge database (measurements recorded by Brest tidal gauge)*

### 4.2.3 Historical skew surges

Historical skew surges are collected through a deep investigation on several sources. Historical skew surges are punctual numerical values of skew surges that are not associated to any time series of water levels recorded by the tidal gauge.

In this application, only the 14 historical data recovered in 3 different sites (La Rochelle, Dieppe and Dunkirk) during the first part of this PhD are considered. The additional 17 historical skew surges founded by Florian Regnier during his internship at EDF R&D LNHE in 2017 are not taken into account. This allows a correct comparison between results of this application and results of previous studies (e.g. the study presented in the Annexe A). In addition, the most of these 17 historical skew surges are recovered in locations in which any time series of systematic skew surges is available and, for this reason, not all of them could have been exploitable in this study.

However, although the 14 historical data considered may not seem a large number of additional data, their contribution in statistical analysis of extreme events can be considerable. When historical data are available, it is unusual to get directly the skew surge value from documentations. For this reason, maximum sea level and the associated maximum astronomical tide have to be known in order to compute the skew surge corresponding to the event of the past period.

In particular, the studies of Garnier and Surville (2010), Gouriou (2012) and Brehil (2014), performed on the collection or on the modelling of historical events at the site of La Rochelle, allow the recovering of 9 historical skew surges (Tab. 1) that are added to the time series of systematic skew surges (Fig. 11).

Gouriou (2012) recovered in archives of the tidal gauge at La Rochelle the 4 oldest historical skew surges (1866, 1867, 1869 and 1872). The historical skew surges of 1924 and 1940 are instead computed through the study of Garnier and Surville (2010). In fact, this study provides the maximum water level and the maximum astronomical tide for the two events of the past.

The three most recent historical events recovered at La Rochelle (1941, 1957, 1999) are calculated by numerical simulations (Brehil, 2014). Fig. 11 and Tab. 1 illustrate the historical skew surge happened on 27$^{th}$ December 1999 (Martin storm) that is computed by the difference between maximum water level and predicted max tidal level provided by Brehil, 2014. This is the biggest skew surge never seen at La Rochelle. Unfortunately, the tidal gauge located in La

Rochelle has not operated in that day. Despite several questions are asked on the truthfulness of this large value, the historical skew surge of 2.17 meters is considered in this application.

Fig. 11 shows these 9 historical skew surges (the green crosses) in the time series of systematic skew surges at La Rochelle. Historical skew surges are isolated data points and, for this reason, the historical period of observations, or better said, what it is happened before or after these historical events is unknown.

| Historical skew surges – La Rochelle | | | | | | | | |
|---|---|---|---|---|---|---|---|---|
| *11 Jan. 1866* | *27 Jul. 1867* | *20 Jan. 1869* | *10 Dec. 1872* | *9 Jan. 1924* | *16 Nov. 1940* | *16 Feb. 1941* | *15 Feb. 1957* | *27 Dec. 1999* |
| **1.11 m** | **0.8 m** | **0.87 m** | **0.96 m** | **1.27 m** | **1.49 m** | **1.37 m** | **1.11 m** | **2.17 m** |

*Tab. 1 – Historical skew surges recovered at the site of La Rochelle*

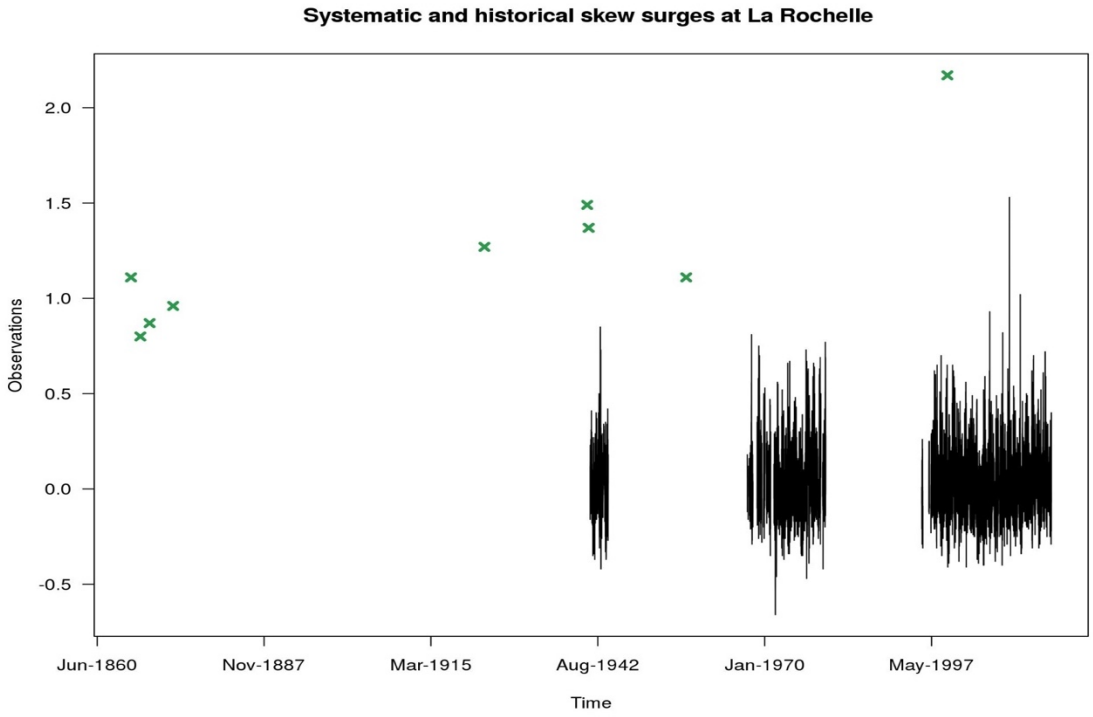


*Fig. 11 – Systematic skew surge recorded by the tide gauge at La Rochelle (in black)and historical skew surges (in green) recovered for La Rochelle*

The technical report of the project NIVEXT (Daubord et al., 2015) provides the only one historical value of skew surge recovered at the site of Dieppe (Tab. 2). As done before for La

Rochelle, this historical skew surge is added to the time series of systematic skew surges recorded by Dieppe's tidal gauge (Fig. 12).

| Historical skew surges | | | | |
|---|---|---|---|---|
| **Dieppe** | **Dunkirk** | | | |
| *17 Dec. 2004* | *29 Nov. 1897* | *1 Mar. 1949* | *1 Feb. 1953* | *2 Jan. 1995* |
| **1.3 m** | **1.75 m** | **1.56 m** | **2.22 m** | **1.18 m** |

*Tab. 2 - Historical skew surges recovered at the site of Dieppe and Dunkirk*

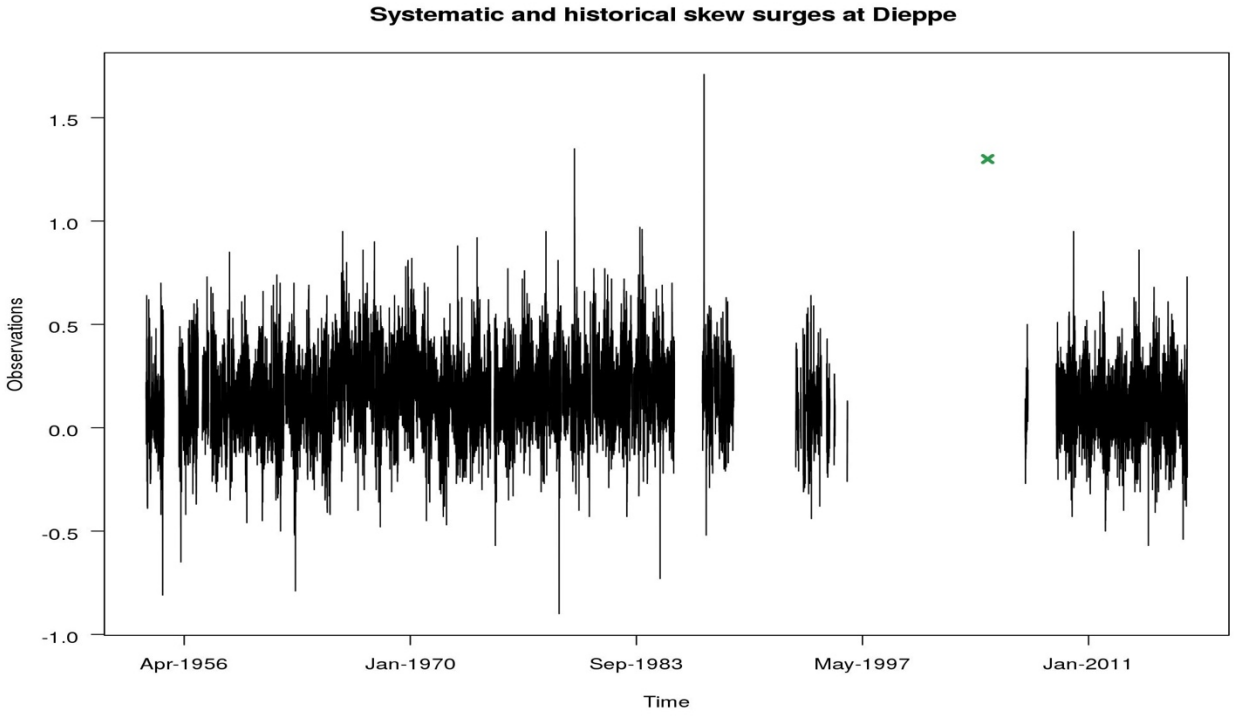


*Fig. 12 - Systematic skew surge recorded by the tide gauge at Dieppe (in black) and historical skew surges (in green) recovered for Dieppe*

On the contrary, several documents are available for the site of Dunkirk. Four additional historical events, are taken into account in this application (Tab. 2). In particular, Dunkirk was impacted by storms in 1897, 1949, 1953 and 1995 that provoked significant skew surges. All of these skews surges are collected by different sources.

Le Cornec and Peeters (2009) state that the maximum water level reached 7.36 meters at Dunkirk on the 29th November 1897 (the municipal archives of Dunkirk is the primary source). The SHOM provides astronomical tide values for many locations by the website "*maree.shom.fr*". Astronomical tides calculated at Dunkirk by the SHOM for that day are equal to 5.71 and 5.78 meters. Making the assumption that the eustatism is the same computed by Weiss (2014) for the period 1956-2010 (1.5 mm/year), the historical skew surge of 1.75 meters is considered.

Le Gorgeu and Guitonneau (1954) state that the maximum sea level of 7.3 meters was reached on the 1st March 1949 at Dunkirk. The associated astronomical tides of 5.77 and 5.83 meters is provided by the SHOM website. Taking into account the eustatism of 1,5 mm/year at Dunkirk (Weiss, 2014), the historical skew surge of 1.56 meters has been computed.

The historical skew surge of 2.22 meters (including the eustatism) has been founded at Dunkirk on the 1st February 1953 by an internal study performed in the past at EDF R&D. This value was already used as systematic skew surge by Weiss (2014). However, a different value of skew surge (2.13 meters) has been used by Bardet et al. (2011) for this event.

Maspataud (2011) evaluates a skew surge of 1.15 meters at Dunkirk on 2nd January 1995 (primary source is Service Maritime de Nordn-S.I.L.E.-Les Dunes de Flandres). Considering the same eustatism of Weiss (2014), the historical skew surge of 1.18 meters is considered.

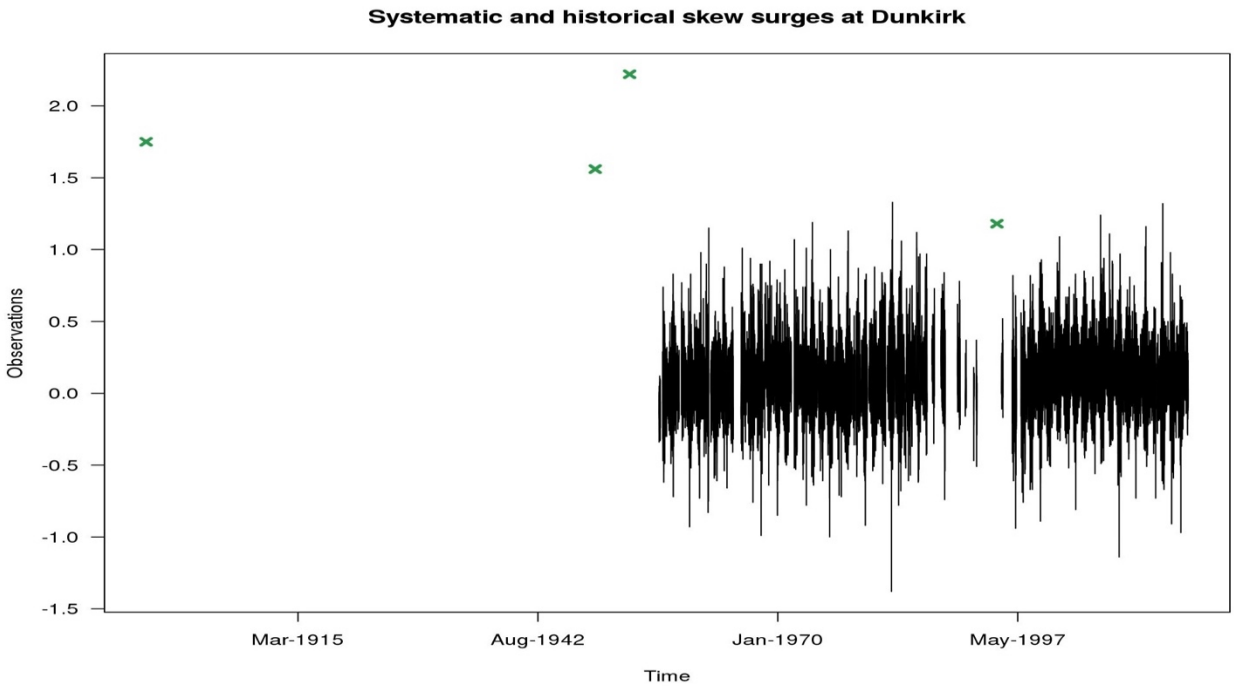


*Fig. 13 - Systematic skew surge recorded by the tide gauge at Dunkirk (in black) and historical skew surges (in green) recovered for Dunkirk*

The historical skew surges recovered at Dunkirk are merged with time series of systematic skew surges recorded by tidal gauge located at Dunkirk (Fig. 13).

Even if for historical skew surges computed at Dunkirk the eustatism calculated for the period 1956-2010 is taken into account, historical skew surges calculated at La Rochelle are not corrected by a likely eustatism. In fact, no information is known about a possible correction already done (mainly for the 3 historical skew surges originated by numerical models). The consideration of an eustatism calculated between 1941-2010 (Weiss, 2014) for many events of the past (exactly 4 of 9 events founded) happened in 19$^{th}$ century could not be proper. For these reasons, historical skew surges recovered at La Rochelle have not been corrected by any eustatism.

The eustatism is not taken into account for the historical skew surge at Dieppe because, being a skew surge quite recent, the eustatism is considered as negligible.

Notwithstanding a complete documentation of past events is provided by authors of scientific studies, historical numerical values must be constantly criticized because the value recovered not always is the correct one. In particular, historical skew surges of the 19$^{th}$ century precise to the centimeter could called into question. In addition, some historical skew surges recovered at Immingham and Portsmouth by other sources for some events happened after the year 2010 had different numerical values compared to the new systematic skew surges computed at these sites (the difference is of few centimeters).

For these reasons, these 14 historical skew surges recovered have been validated as proposed in Chapter 2. For the moment, any validation has been performed for these events.

# 4.3 Physical homogeneous regions

Physical homogeneous regions are formed in FAB method by a process based on the computation of probabilities $p_{ij}$ that storms occurred in a site $i$ might impact also the site $j$ and vice versa.

This method to form homogeneous regions is the same proposed in the RFA approach. In this approach, the process to form regions was principally developed for continuous time series of modelled significant wave heights in which data are observed for a common period in every site. When data come from different tide gauges, the recording period can be not the same in each location.

For this reason, the probabilities $p_{i,j}$ that a storm impacts the site $i$ and the site $j$ for a same storm have to be computed for a period in which the most part of tide gauges are operating. A particular period has to be defined to form homogeneous regions. This allows the optimisation of formation of physical homogeneous regions. In addition, a sensitivity analysis on the three parameters that lead the formation of physical region is recommended. Further details are illustrated in the following.

All the probabilities $p_{ij}$ should be ideally computed from data approximately recorded for a same period of time at each site in order to form accurate typical storms footprints and consequently precise physical regions. More time periods of tide gauge recordings from different sites are common, more the probabilities $p_{ij}$ are less impacted by mutual time periods of data and they could be properly hierarchically compared and clustered. In fact, hierarchical clustering method provides better typical storm footprints if applied to probabilities $p_{ij}$ that are computed for approximately the same period of time. Computing probabilities $p_{ij}$ for a same time period at each site is possible only when dealing with modelled time series that are generated for a same time period.

In this application, skew surges are available in 74 tide gauges that start and finish to operate in different periods. In addition, they have different periods of failure on gauging. For this reason, a time window in which most of tide gauges operate has to be chosen in order to estimate proper values of $p_{ij}$ and to get accurate physical homogeneous regions.

Fig. 14 illustrates the number of working tide gauges during every year. Tide gauges never work at the same time.

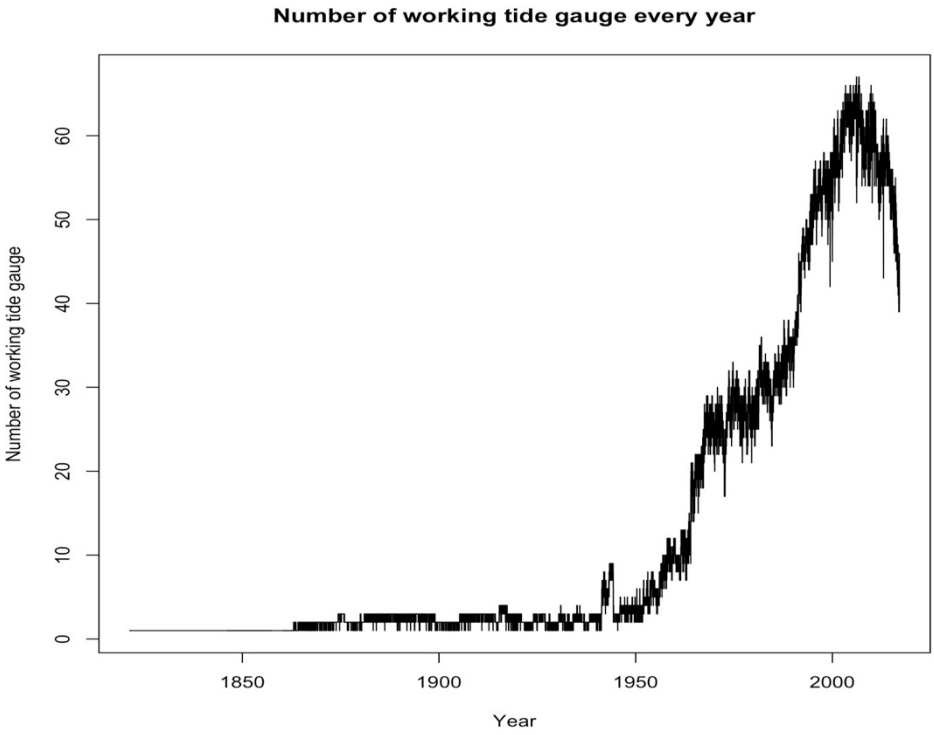


*Fig. 14 – Number of operating tide gauges per year*

A clear breaking point on the number of working tide gauges is marked between the beginning and the end of the year 1950. In fact, the most part of the 74 tide gauges available in this database starts to operate and to measure water levels from the beginning of the year 1950. For this reason, the time window in which the probabilities $p_{ij}$ are considered to form physical homogeneous regions lasts 67 years (from 1951 to 2017). In this time window approximately 35 of 74 tide gauge are operating on average.

Another shortest time window with more tide gauges operating on average could be chosen but it is important to specify that more the time window is reduced and more the probabilities $p_{ij}$ might be inaccurate. On the contrary, the extension of the time window before 1951 would mean that the probabilities $p_{ij}$ are computed also for time periods in which only 2 tide gauges work on average.

In this application, typical storm footprints are computed only for storms occurred after the 31$^{st}$ December 1950.

A generic site *i* must typically have a computing occurrence probability between all other interested sites in order to use a hierarchical method. In fact, if a site *i* has not common period

with a site $j$, the probability $p_{ij}$ cannot be computed. Unfortunately, 5 of our 74 sites face with this problem. These 5 sites are removed when hierarchical clustering method is applied.

After the formation of physical regions, they can be reintroduced in the region in which they evidently belong. In this study, the sites removed are Saint-Servan, Dielette, Le Crouesty, Port Bury and Moray Firth. A particular case arises for the site of Le Crouesty. Removing the other 4 sites, the site of Le Crouesty have any common period with the site of Le Verdon. A choice of which site had to be removed is carried out depending on length of time series. Tide gauge at Le Verdon operates for the most part of the years between 1951-2000 and until to November 2000 while the tide gauge at Le Crouesty starts the recordings from the end of the year 2000.

A test removing the site of Le Crouesty instead of the site of Verdon is performed at the end of this analysis. Using the parameters for storm clusters chosen in the following, the physical homogeneous regions are precisely the same of that founded in this application (Fig. 21).

#### 4.3.1.1 Parameters to detect storms

The formation of physical homogeneous regions is applied only to storms occurred after the year 1950. Notwithstanding, storm clusters have to be created for all the available events. In fact, the determination of clusters for all the events is necessary to define the regional extreme data samples composed by all extreme events occurred in the considered region.

Physical storms are detected by a spatiotemporal declustering and they are defined by three parameters ($p$, $\Delta$, $\eta$). Extremes happened in neighbour sites $\eta$ during a temporal interval $\Delta$ are generated by the same storm. In particular, two or more extreme values that exceed the local physical threshold (represented by the $p$-value) belong to the same storm if they occur in $\eta$-nearest sites during an interval of $\Delta$ hours.

The value of 0.995 is widely used in literature of extreme events (Mendez et al., 2008; Di Baldassarre et al., 2009; Laio et al., 2009; Weiss, 2014) for the parameter $p$ and, for this reason, a sensitivity analysis on the other two parameters $\Delta$ and $\eta$ is performed.

The variation of these two parameters could generate significant differences in the formation of storm clusters. This would impact the formation of physical and statistical homogeneous regions and successively regional and local estimations of extreme events. In fact, storm clusters are physical element that represent an effective storm. The goodness of representation of its

physical process depends on the parameters used to form clusters. For this reason, a sensitivity analysis on these parameters that generate storm clusters have to be performed.

The same sensitivity analysis is recommended for each application of the FAB method to databases of variables recorded in different locations.

**Sensitivity analysis for the temporal parameter $\Delta$**

Before to perform the analysis performed for the temporal parameter $\Delta$, it is important to recall that the identification of a valid temporal parameter $\Delta$ is necessary to get a satisfactory representation of storms. In particular, a single storm can be identified like two or more different storms if the value of $\Delta$ hours is too little and, on the contrary, if the value of $\Delta$ hours is excessively high, two or more different storms can be identified as a single one.

For this reason, three different values of temporal parameter $\Delta$ hours are considered to detect storms in this application. This analysis is performed separately for storms happened before the year 1951 that are not used on the process of formations of physical regions and for storms occurred after the year 1950. In fact, as a result of the previous study (Fig.3), the duration of a storm propagation $\Delta$ has to be higher when only few tide gauges operate. More time is needed to a storm moving to another operating location that it should ideally be more far. For this reason, storms happened before the year 1951 and after the year 1950 are independently analysed.

In particular, the duration of a storm, or better the difference in time between the first and the last extreme event of a storm cluster, is examined for the three different values of $\Delta$ hours: 25 hours, 48 hours and 72 hours. A value of 25 hours instead of 24 hours is considered to allow the realisation of a time of at least two tidal cycles in a same location. Histograms of number of storms for 12 hours' progressive intervals of storm durations are produced to interpret easily the results of this sensitivity analysis.

The results of this analysis are illustrated below for a spatial parameter of $\eta=16$. In any case, analyses with other spatial parameters have been performed. Behaviours of histograms with other spatial parameters are similar to these of Fig. 15 and Fig. 16.

A $\Delta$ of 25 hours is selected as the most satisfactory value by the analysis performed for storms happened after the year 1950. In fact, as the histograms of Fig. 15 and Fig. 16 shown, more the value of $\Delta$ hours is higher and more the storms have a longer duration. The histogram for a $\Delta$ of 72 hours (on the right side of Fig. 16) illustrates that more than 50 storms of the 1036 storms detected in total last more than 6 days and two storms last approximately 25 days. The detection of a storm that lasts 25 days has not any physical sense. Similar considerations can be pointed out for the case of a $\Delta$ of 48 hours in which 1189 storms are detected. This case is illustrated in the histogram on the left side of Fig. 16.

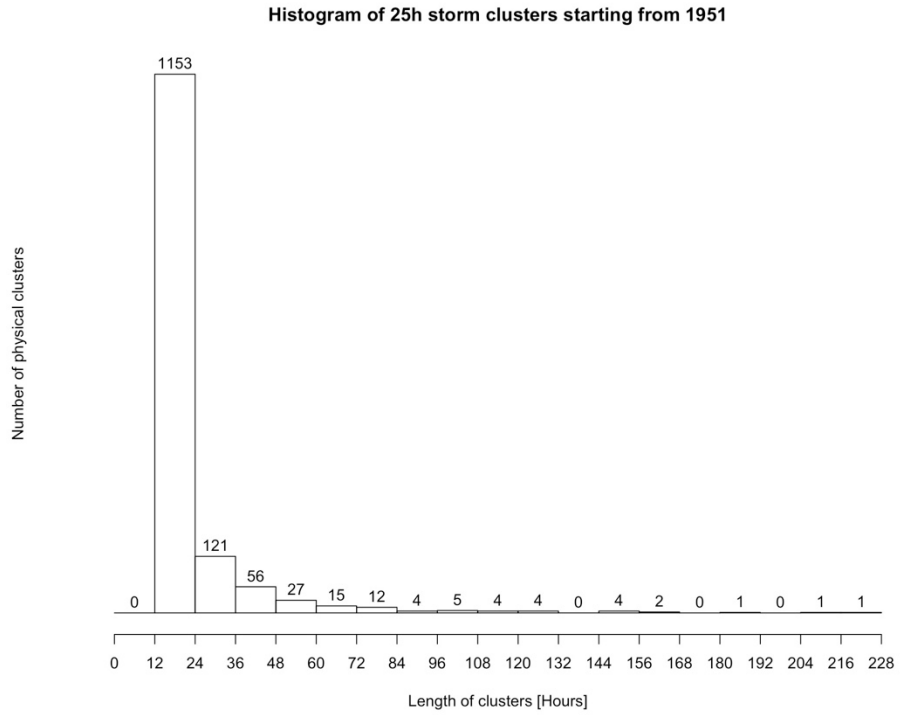


*Fig. 15 – Histogram of the number of storm clusters created by a $\Delta$=25 hours and a $\eta$=16 in function of their storm duration (in hours) for storms happened after the year 1950*

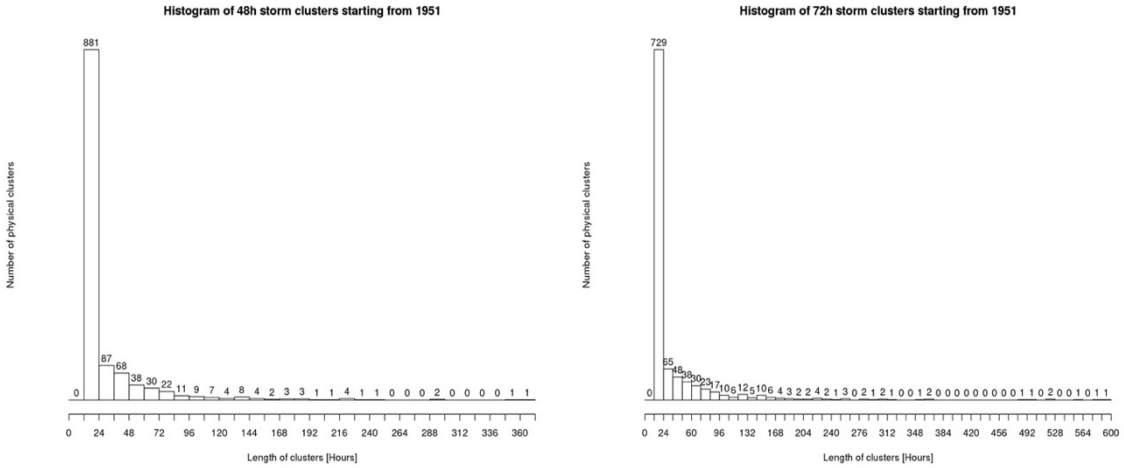


*Fig. 16 - Histograms of the number of storm clusters created by a Δ=48 hours (on the left) or a Δ=72 hours (on the right) and a η=16 in function of their storm duration (in hours) for storms happened after the year 1950*

Conversely, for a $\Delta$ of 25 hours, only 9 storms of the 1410 detected last more than 6 days and, in addition, the biggest one lasts 9 days. A temporal parameter $\Delta$ of 25 hours can be considered satisfactory for this application and it is used to detect storms happened after the year 1950.

The same analysis is performed for storms occurred before the year 1951 (Fig. 17 and Fig. 18).

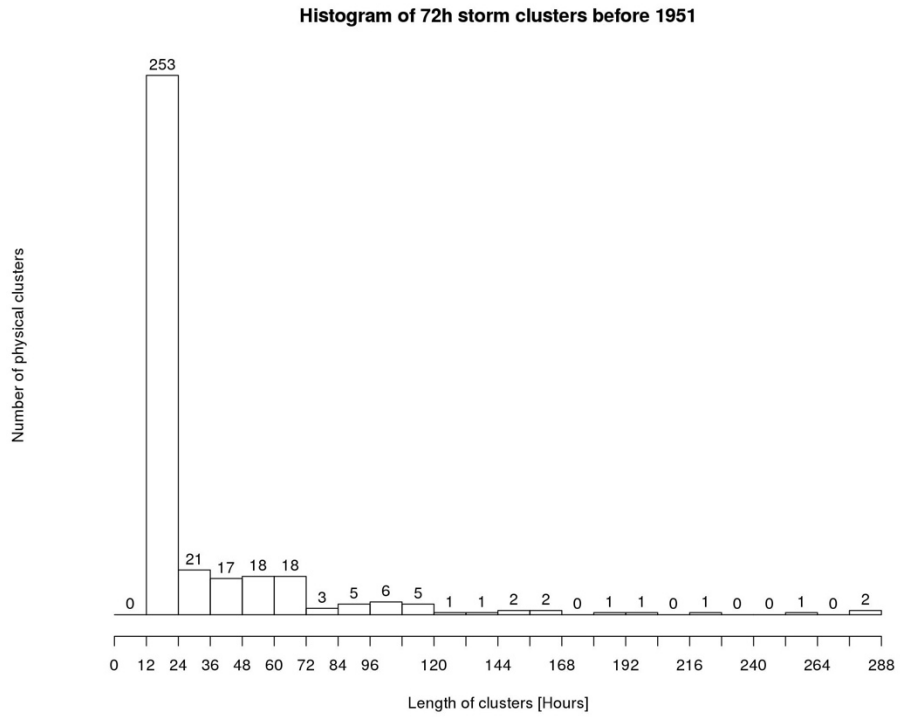


*Fig. 17 - Histogram of the number of storm clusters created by a Δ=72 hours and a η=16 in function of their storm duration (in hours) for storms happened before the year 1951*

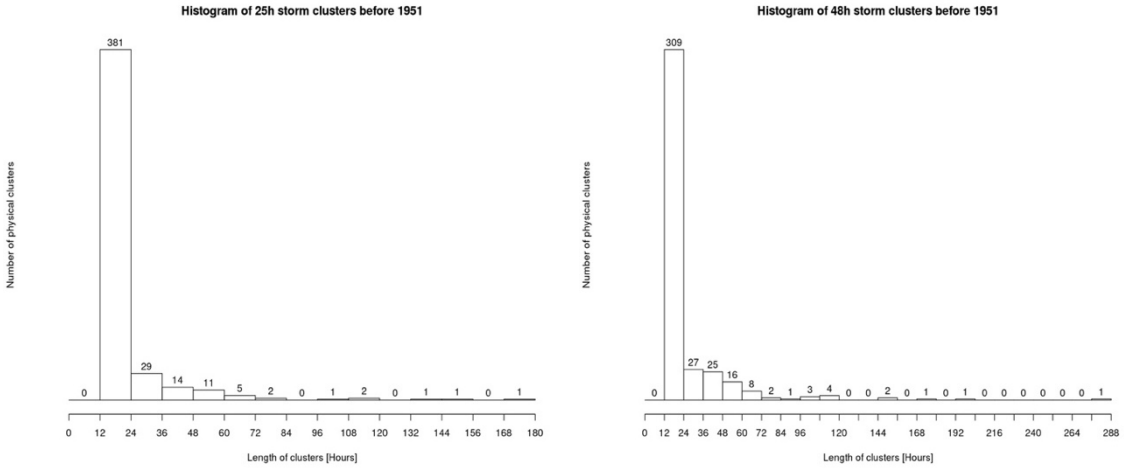


*Fig. 18 - Histograms of the number of storm clusters created by a $\Delta$=25 hours (on the left) or a $\Delta$=48 hours (on the right) and a $\eta$=16 in function of their storm duration (in hours) for storms happened before the year 1951*

During the years before the 1951, only few tide gauges operate. The sensitivity analysis of the temporal parameter $\Delta$ is performed for values of 25 hours, 48 hours and 72 hours. The histogram for a $\Delta$ of 25 hours (on the left side of Fig. 18) shows that 381 storms of 448 detected last less than 1 day. In addition, only a few number of storms has a duration higher than 48 hours. On the contrary, the histogram created for a $\Delta$ of 48 hours (on the right side of Fig. 18) and 72 hours (Fig. 17) shown as the storm duration is more uniform. A shorter percentage of storms for these two cases last more than 1 day and only few storms last more than 6 days (the biggest one lasts approximately 10 days). Notwithstanding both cases give satisfactory results, a $\Delta$ of 72 hours is considered for storms occurred before the 1951 to give a sufficient time to a storm to be detected to a farther operating location. Finally, storms happened before 1951 are created for a $\Delta$ of 72 hours.

These results obtained by this sensitivity analysis confirm that the division performed for extreme storms before the year 1951 and after the year 1950 had to be performed. In periods of time with less working tide gauges, the $\Delta$ value is higher than in time periods in which several tide gauges work.

**Sensitivity analysis for the spatial parameter $\eta$**

The choice of a valid temporal parameter $\Delta$ of 25 hours for the storms occurred after the year 1950 allows the performance of the sensitivity analysis for several values of the spatial parameter $\eta$. In particular, a stability on the composition of physical regions is investigated. A valid $\eta$ value is important to detect correctly a storm.

A same storm can be detected as two or more different storms if the spatial parameter $\eta$ is a little value. On the contrary, two or more storms can be detected as a single storm if the spatial parameter $\eta$ is assumed as a high value.

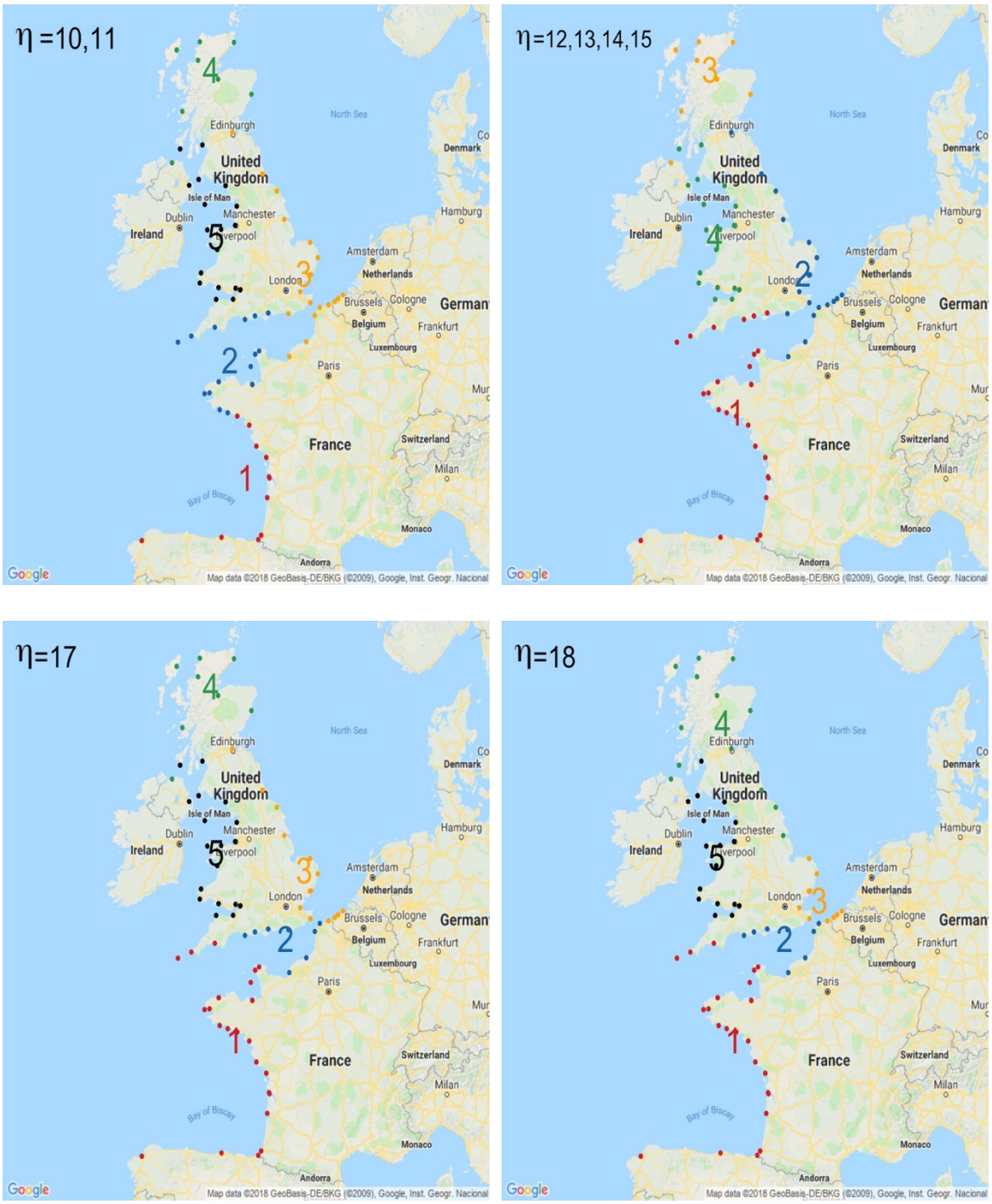


*Fig. 19 – Physical regions formed for different values of the spatial parameter η (10,11,12,13,14,15,17,18) around the value parameter of η=16 selected and using the selected temporal parameter Δ of 25 hours. Source of the map: Google Maps*

Several compositions of physical regions are obtained varying the spatial parameter $\eta$ between 10 and 18. These 9 cases are considered in this analysis. The $\eta$ value has to be a value neither too big and nor too small compared with the total number of available locations.

Fig. 19 figures out the compositions of the physical regions for these different values of $\eta$. For a spatial value between 12 and 16, the composition of physical regions is the same. The higher parameter $\eta$ between 12 and 16 is considered for this study as the valid spatial parameter that provides more extended clusters.

The spatial parameter $\eta$ of 16 nearest sites is used for the formation of storm clusters happened before and after the year 1950. Storm clusters are formed in this study for the following parameters: $p=0.995$, $\eta=16$ and $\Delta=72$ *hours* or $\Delta=25$ *hours* depending respectively on the period of the event: the first value of the parameter $\Delta$ is used for storms before the year 1951 and the second value of the parameter $\Delta$ for storms after the year 1950.

### 4.3.1.1 Physical homogeneous regions

The formation of storm clusters of skew surges enables the formation of physical homogeneous regions. The method to form physical regions is the same used in the RFA approach.

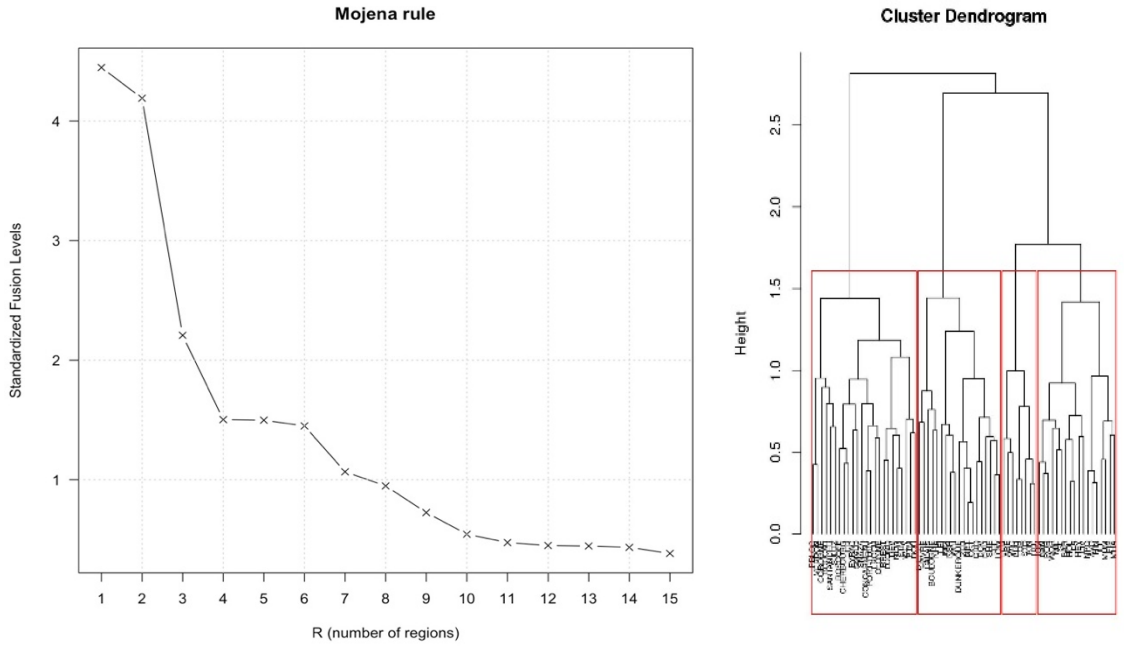


*Fig. 20 – The graph of the Mojena's stopping rule (on the left) and the cluster dendrogram (on the right)*

The probabilities $p_{ij}$ are computed for storms occurred after the year 1950. The resulting dissimilarity indexes $d_{ij}$ can be now estimated. The hierarchical clustering method proposed by Ward (1963) is performed in order to select the most typical configuration of storms' footprints through the most significant jump of the dendrogram heights (Mojena, 1977). For this application, the most significant jump of the Mojena's stopping rule is obtained for 4 regions (Fig. 20).


*Fig. 21 – The 4 physical homogeneous regions founded by the typical storm footprints for events happened after the year 1950. Source of the map: Google Maps*

Four physical homogeneous regions are thus formed for the 74 sites of the skew surges' database (Fig. 21). The composition of the physical regions is similar to that calculated by Weiss (2014) of Fig. 22 and to the typical storms' footprints obtained by Haigh et al. (2016) for the extreme events of the SurgeWatch database.

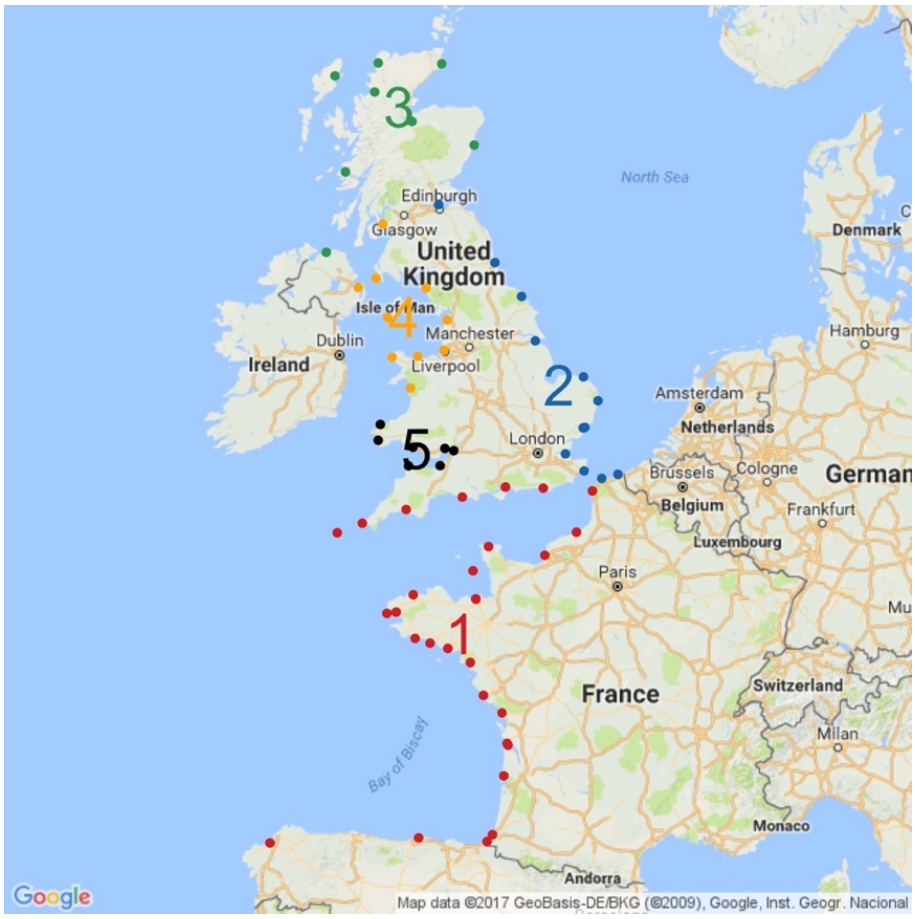


*Fig. 22 – The five physical and statistical regions founded in the PhD thesis of Weiss 2014*

In particular, Weiss (2014) obtained in his study 5 physically and statistically homogeneous regions (Fig. 22) selecting $p=0.995$, $\Delta=24h$ and $\eta=14$ as valid parameters. These values are founded by Weiss (2014) after an analysis on the biggest storms well-known as, for instance, the Lothar and Martin storms that impact principally coasts of the Bay of Biscay between 26$^{th}$ and 28$^{th}$ December 1999.

However, the statistical threshold of a particular site is higher compared with its physical threshold. Statistical thresholds have to be chosen in such a way to get a $\lambda$ extreme values on average each year in every site. For this reason, local statistical thresholds are computed fixing a common $\lambda$ value for all sites of the region. A value of $\lambda=1$ has been used in the RFA application for skew surges by Weiss (2014) in all the five regions.

The slight differences in the composition of physical regions obtained in the FAB application and the RFA application performed by Weiss (2014) impact especially the sites located in the English Channel. Different borders between the Region 1 and the Region 2 are caused by the

introduction of the three Belgian sites that extend the Region 2 and by the correction of the R function "*hclust*" used previously by Weiss (2014) to apply the hierarchical clustering method of Ward (1963). In particular, Murtagh and Legendre (2014) affirm that the R function '*hclust*' must be used with squared Euclidean distances $d_{ij}$ to implement correctly the Ward method. In this application, squared distances $d_{ij}$ are properly used.

# 4.4 Computation of optimal sampling threshold

In the FAB method's application, the optimal $\lambda$ is the results of the analysis of all the more important parameters of the regional analysis. In particular, it is selected through a weighting analysis as the best $\lambda$ case between 176 different $\lambda$-cases. The optimal $\lambda$ case corresponds to a regional extreme data sample that satisfies all the primary tests and has obtained the best global weighting value on secondary parameters.

In this application, physical homogeneous regions containing sites with available historical data are considered. Historical skew surges are available for three sites: La Rochelle located in the Region 1 and Dieppe and Dunkirk in the Region 2.

For this reason, the primary tests are performed in the regional extreme data sample of Region 1 and Region 2 for every $\lambda$ value between 0.25 to 2 by steps of 0.01. The 176 $\lambda$-cases for each region are analysed. Only $\lambda$-cases verified are successively used for the weighting analysis of secondary parameters.

Depending on the $\lambda$ value, these parameters are computed in the frequentist analysis' case for the Region 1 (Fig. 23) and for the Region 2 (Fig. 24).

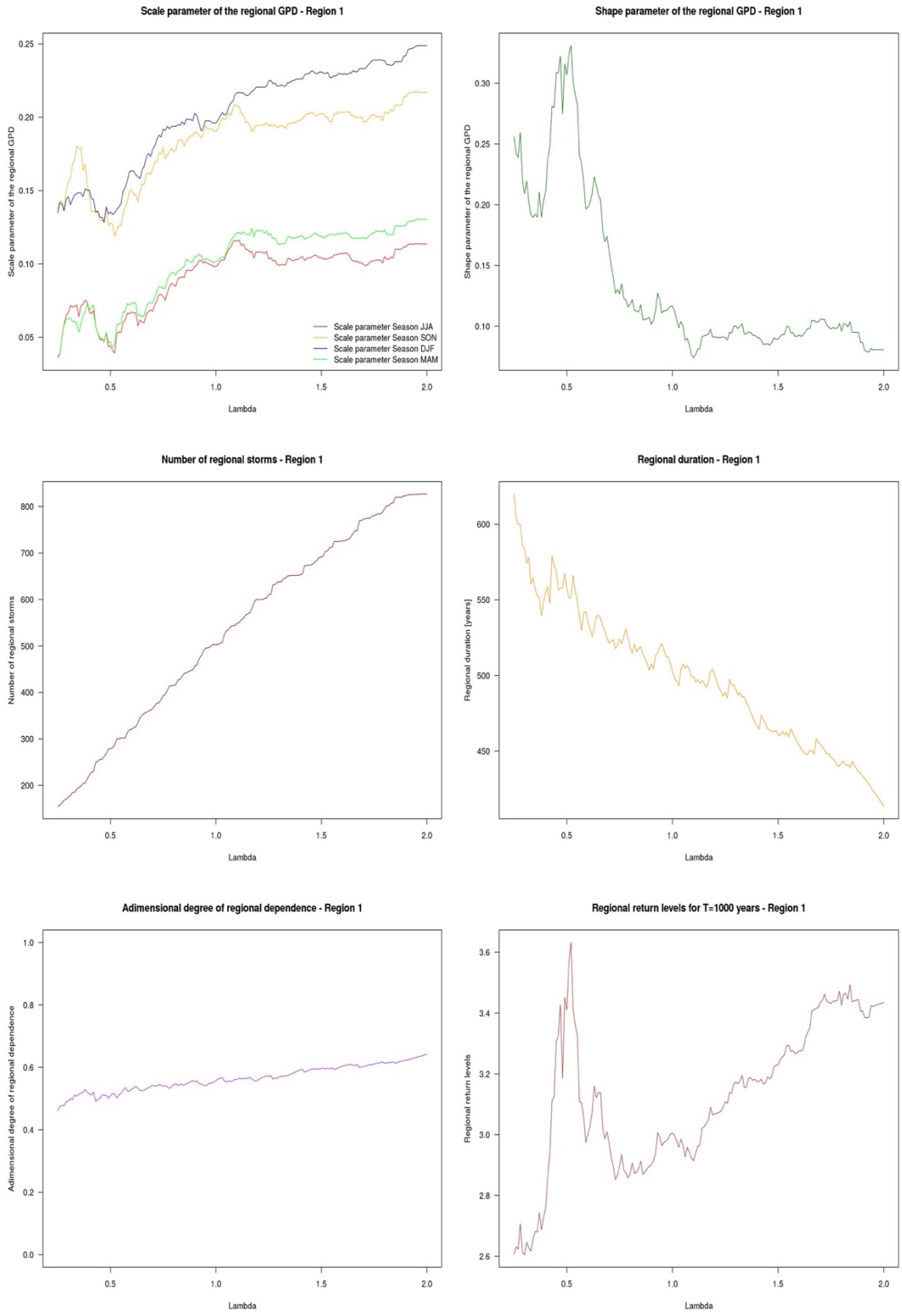


*Fig. 23 – Sensitivity analysis of secondary parameters used for the Region 1*

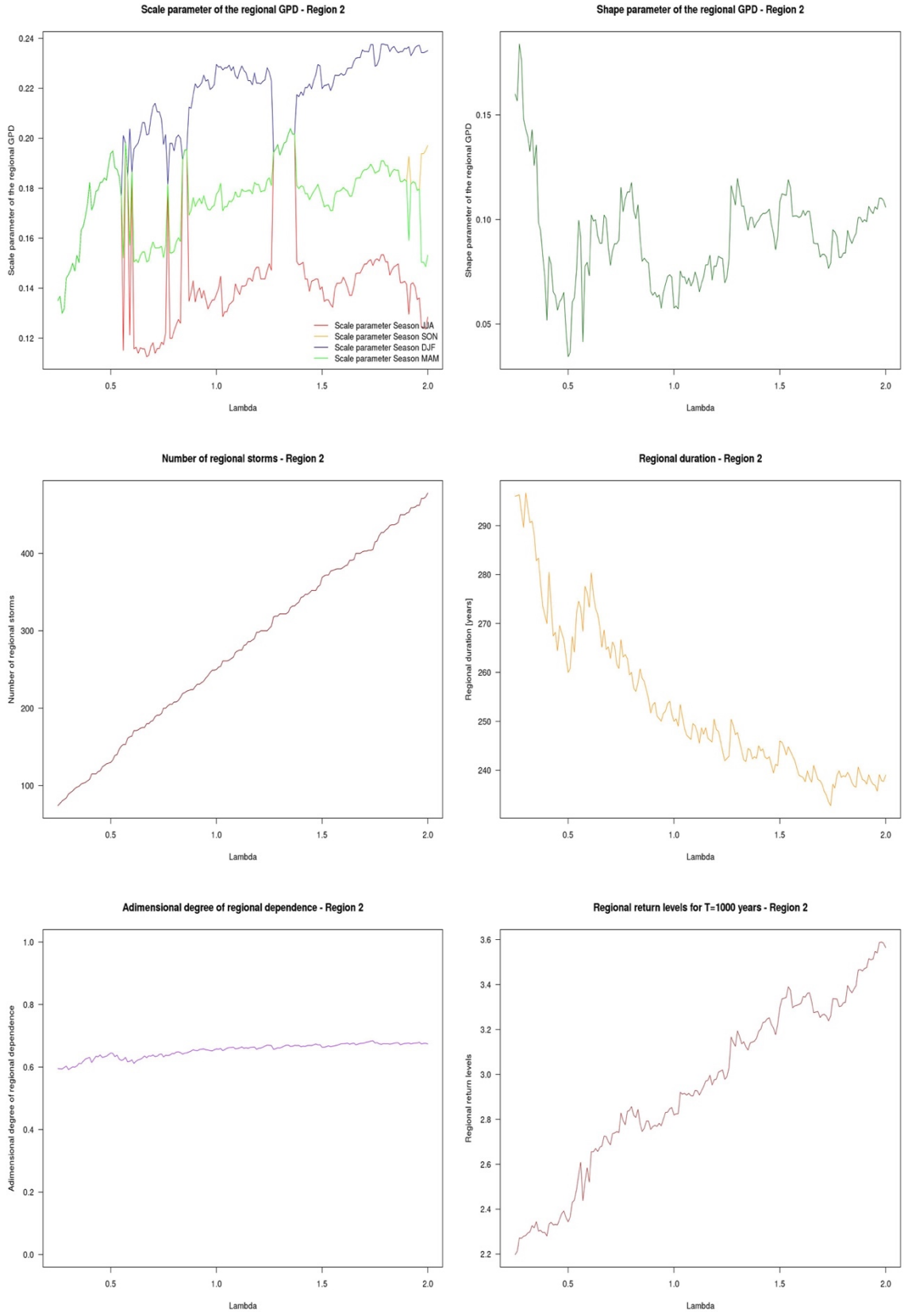


*Fig. 24 – Sensitivity analysis of secondary parameters used for the Region 2*

Furthermore, secondary parameters are computed for the Bayesian analysis' case for the Region 1 and for the Region 2 through the use of the "*nsRFA*" R package. This package enables the solving of the MCMC algorithm and the computation of the posterior distribution of the regional GPD parameters.

In the Bayesian case, same types of primary and secondary parameters are used. All the five primary parameters proposed do not depend on the framework of the statistical analysis. On the contrary, three of the seven secondary parameters are differently estimated in the two statistical framework of analysis: the two regional GPD parameters and the regional return levels linked to a return period *T* of 1000 years. In particular, the mode of the *U=100000* iterations of regional GPD parameters' vectors θ is computed for each value of $\lambda$ between 0.25 and 2 (Fig. 25 and Fig. 26). Standard estimative regional return levels linked to a return period *T* of 1000 years can be now computed for each value of $\lambda$.

These return levels could correspond to that computed in frequentist context for a PMLE without considering the seasonality of skew surges. In fact, in the particular case in which the seasonality of skew surges is not considered in frequentist estimations, results of primary and secondary parameters are identical for the frequentist and for the Bayesian analysis' cases.

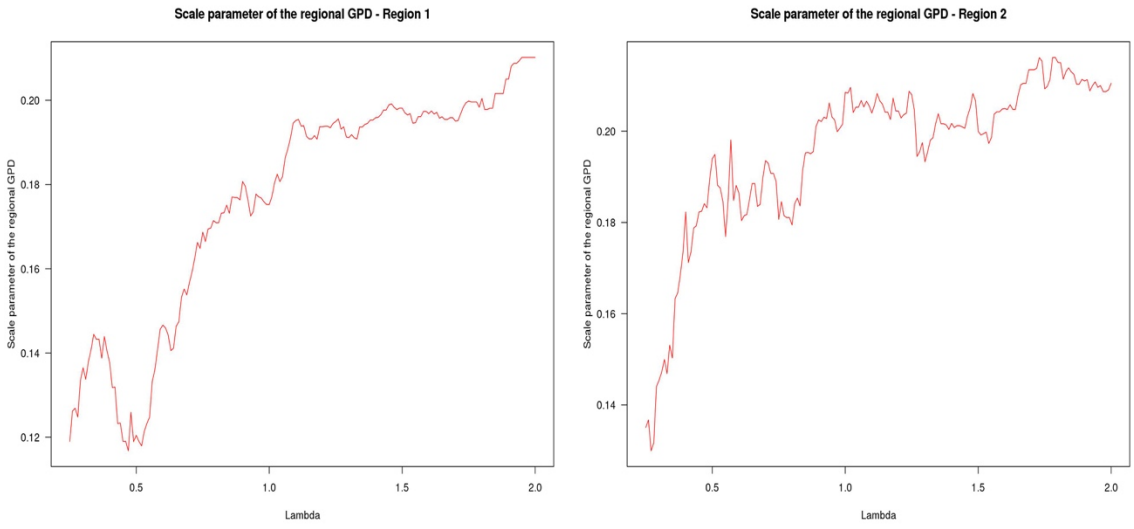


*Fig. 25 – Sensitivity analysis of regional Bayesian scale parameter for Region 1 and Region 2*

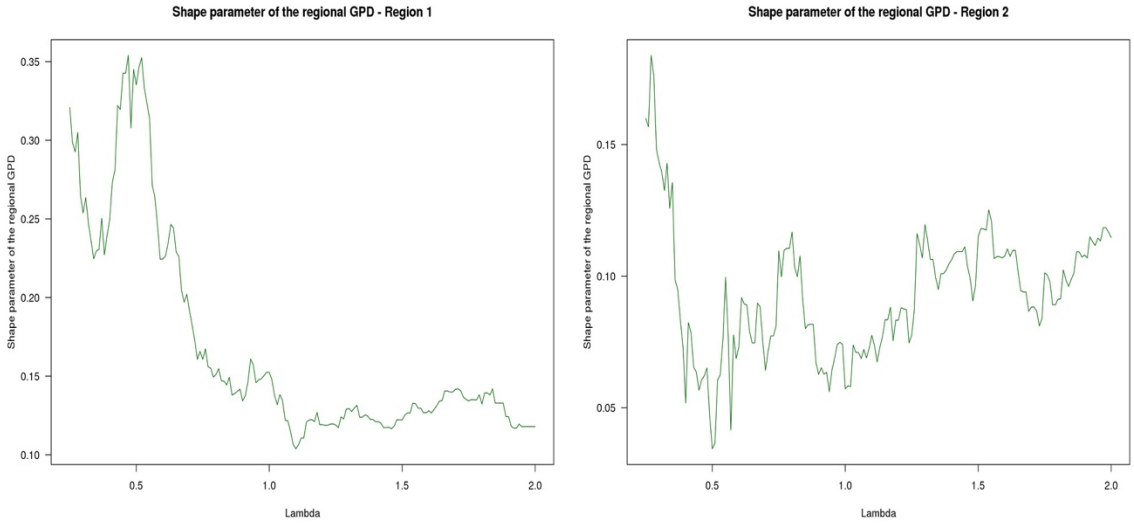


*Fig. 26 – Sensitivity analysis of regional Bayesian shape parameter for Region 1 and Region 2*

The weighting analysis of the secondary parameters provides the same optimal $\lambda$ value for the frequentist and Bayesian cases. In particular, the optimal $\lambda$ value for the Region 1 corresponds to a value of 0.84 storms on average per year and to a value of 1.79 for the Region 2.

A further test is performed for the frequentist case. Using the weighting of the upper value of the regional confidence interval for a return period T of 1000 years instead of the regional return level linked to a return period T of 1000 years. Same optimal $\lambda$ values are identified through this alternative test in both regions.

In any case, a particular clarification has to be provided for the application performed in the scientific publication for NHESS (Annexe A). In that case, the sampling threshold of Region 1 was identified for a $\lambda$ value of 0.36. This $\lambda$ value had been defined after a visual look on a total of twelve parameters for each possible value of $\lambda$. In that case, sensitivity analysis' results had been translated in an optimal value of threshold without the application of an unequivocal approach of computation. In particular, several other values of $\lambda$ can be considered as optimal in that application. That choice was considered the better one to illustrate the benefit of the use of historical data on the regional analysis. Moreover, in the study of Annexe A, the regional analysis was applied to a database of skew surges not yet updated with the three Belgian sites. Physical homogeneous regions were calculated without performing a sensitivity analysis on parameters used to identify the storm clusters.

# 4.5 Physical and statistical regions

The statistical homogeneity of physical regions is verified only for the particular region considered. A physical homogeneous region linked to the optimal $\lambda$ value has already been statistically verified. In fact, the statistical homogeneity test is a primary test and it is already verified for optimal $\lambda$ values. Furthermore, , the statistical homogeneity of all physical homogeneous regions for the optimal values of $\lambda$ obtained by in the previous analysis has to be tested in order to show the definitive map of the physical and statistical homogeneous regions.

For the two optimal $\lambda$, regions except the Region 4 of Fig. 21 are statistically homogeneous. For this reason, a further division into two different sub-regions has to be performed for Region 4. The new sub-regions are retested by the homogeneity test and now they appear as statistically homogeneous. Finally, five physical and statistical homogeneous regions are founded in this study for the both optimal $\lambda$ identified for the Region 1 and the Region 2. The five physical and statistical homogeneous regions are shown by the map of Fig. 27.


*Fig. 27 – Physical and statistical regions for lambda=0.84 and lambda=1.79. Source of map: Google Maps*

# 4.6 Frequentist estimations of return levels

The statistical analysis is performed for the two regional extreme data samples defined for the Region 1 and the Region 2. Estimations of the frequentist return levels are computed for several return periods *T*.

Tab. 3 and Tab. 5 illustrate all the main elements of the regional analysis obtained by the application of the FAB method in a framework of frequentist estimation.

Tab. 4 and Tab. 6 show the results of the regional statistical analysis for the Region 1 and the Region 2. In particular, regional return levels associated to a return period of 1000 years, their upper bounds of the 90% confidence intervals and the percentage of the relative width of these intervals are figure out.

These results are displayed in the return level plots of Fig. 28 and Fig. 29. Confidence intervals are calculated by a bootstrap of $U=10^5$ new regional extreme data samples.

In addition, empirical regional extreme data are positioned in return levels by the use of a Weibull position (Weibull, 1951) in Fig. 28 and Fig. 29. Historical data are displayed by red dots in order to recognise the significance of historical data compared with systematic data. Grey dotted lines are used to illustrate the 90% confidence intervals.

| **Regional parameters of the Region 1** | | | | |
|---|---|---|---|---|
| *Optimal* $\lambda$ | *Scale param. of regional GPD (season DJF)* | *Shape parameter of regional GPD* | *Regional credible duration (years)* | *Adimensional degree of regional dependence* $\Phi$ |
| **0.84** | **0.197** | **0.112** | **517.86** | **0.544** |

*Tab. 3 – Regional parameters computed by the FAB method applied to the Region 1*

| Results for the Region 1 | | |
|---|---|---|
| *Regional quantiles for T=1000ys* | *Regional upper CI 90% for T=1000ys* | *ΔCI90 / yR,T=1000ys (%)* |
| **2.89** | **3.39** | **34** |

*Tab. 4 - Regional return levels computed by the FAB method applied to the Region 1*

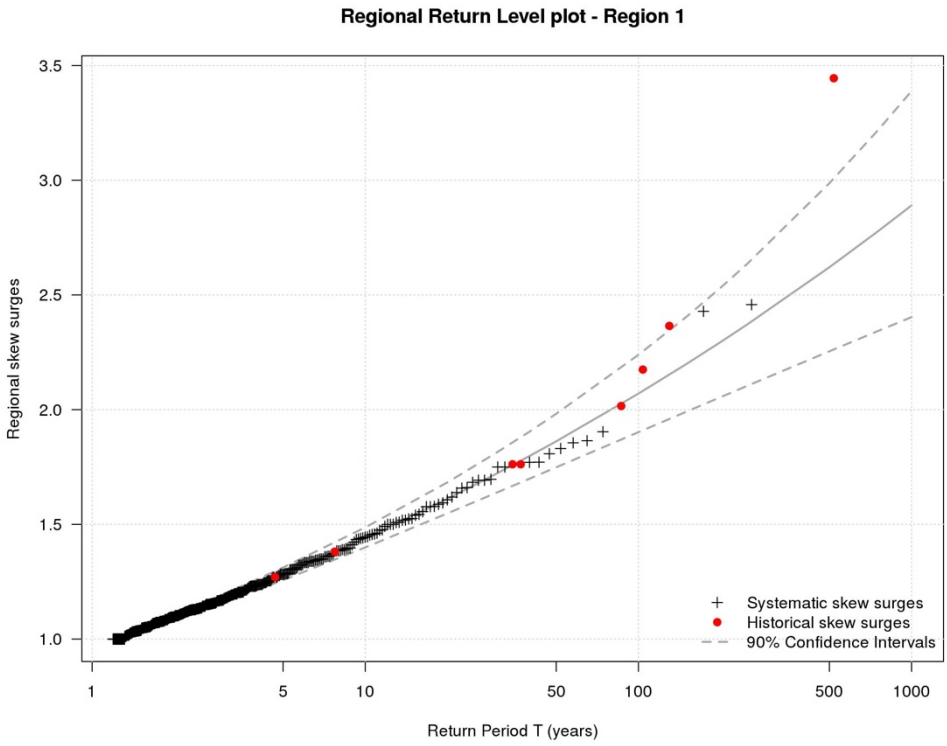


*Fig. 28 – Regional return level plot for the Region 1*

Fig. 28 show the return level plot of the Region 1. The biggest event is represented by an historical data. In particular, it corresponds to the storm that impacts La Rochelle in the year 1999. Notwithstanding this event seems very far from the others, no outliers are detected in this regional extreme data sample.

| Regional parameters of the Region 2 | | | | |
|---|---|---|---|---|
| *Optimal λ* | *Scale param. of regional GPD (season DJF)* | *Shape parameter of regional GPD* | *Regional credible duration (years)* | *Adimensional degree of regional dependence* |
| **1.79** | **0.238** | **0.082** | **238.55** | **0.675** |

*Tab. 5 - Regional parameters computed by the FAB method applied to the Region 2*

| Results for the Region 2 | | |
|---|---|---|
| *Regional quantiles for T=1000ys* | *Regional upper CI 90% for T=1000ys* | *ΔCI90 / yR,T=1000ys (%)* |
| **3.30** | **3.99** | **40** |

*Tab. 6 - Regional return levels computed by the FAB method applied to the Region 2*

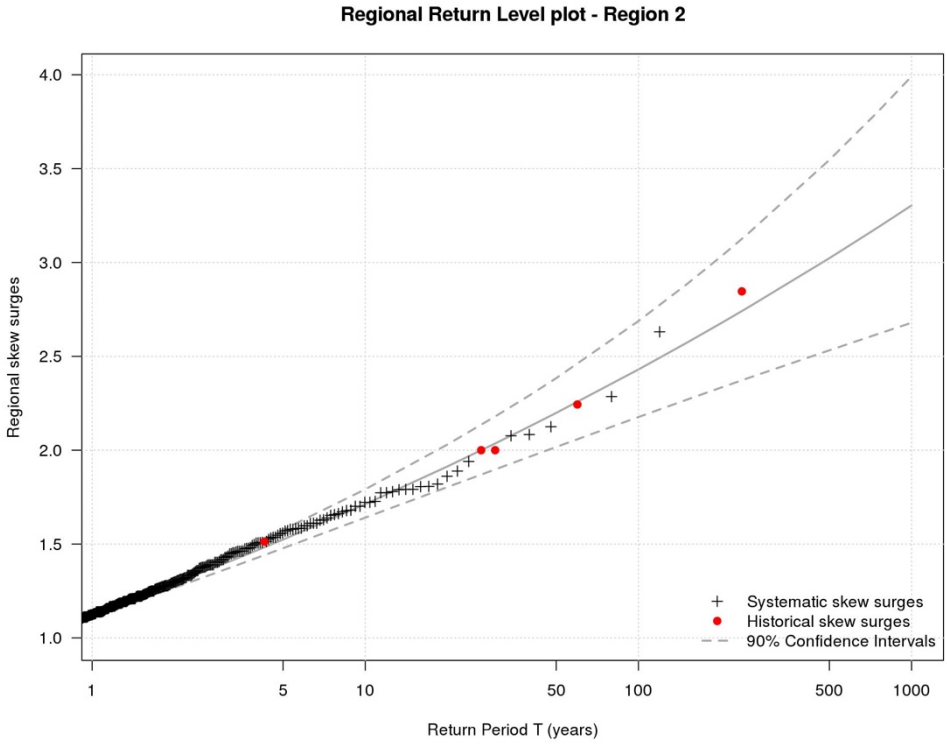


*Fig. 29 – Regional return level plot for the Region 2*

Fig. 29 displays the return level plot of the Region 2 in which the biggest event corresponds to an historical data. In this case, this historical event is located within the 90% confidence intervals.

The use of historical data in the regional analysis could impact differently the local estimations. In fact, sites of a region preserve their local features by local indexes that assume different value in each site. For this reason, two sites (randomly chosen) belonging to the Region 1 (La Rochelle) and to the Region 2 (Calais) are examined in the same way as the regional estimations. Tab. 7 shows their local return levels associated to a return period of 1000 years.

The relative width of the 90% confidence intervals for the site of La Rochelle is little higher than the Region 1. This means that the uncertainties linked to the return levels associated to a return period of 1000 years are bigger at La Rochelle than in this region.

On the contrary, the site of Calais has the same relative width of the 90% confidence intervals of the Region 2.

Local return level plots for these two sites are illustrated in Fig. 30. Empirical regional extreme data are locally calculated by the local index and illustrated in these return levels.

| **La Rochelle** | | | **Calais** | | |
|---|---|---|---|---|---|
| *Quantiles for T=1000ys (meters)* | *Upper CI 90% for T=1000ys (meters)* | *ΔCI90 / xT=1000ys (%)* | *Quantiles for T=1000ys (meters)* | *Upper CI 90% for T=1000ys (meters)* | *ΔCI90 / xT=1000ys (%)* |
| **1.82** | **2.15** | **36** | **1.78** | **2.14** | **40** |

*Tab. 7 - Results for the sites of La Rochelle (Region 1) and Calais (Region 2)*

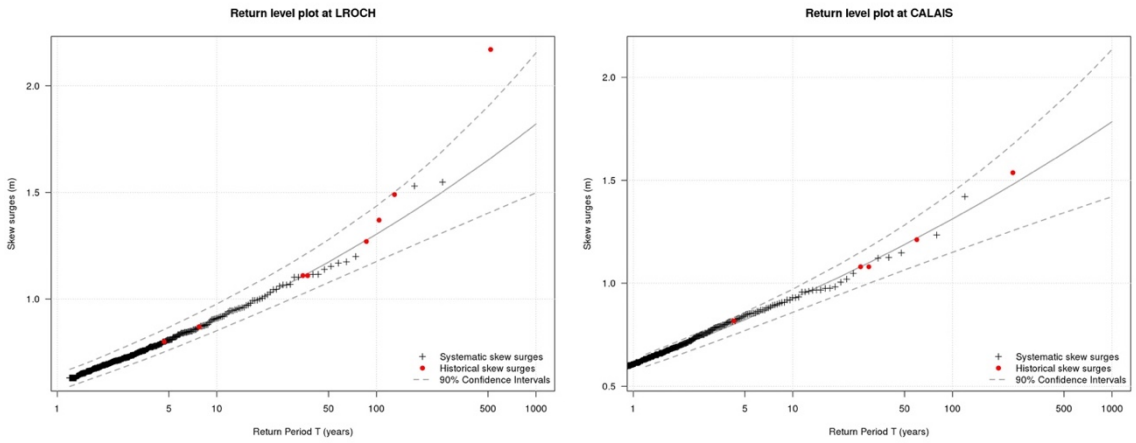


*Fig. 30 – Local return levels plots for the sites of La Rochelle (on the left) and Calais (on the right)*

# 4.7 Estimations without historical data

The same frequentist analysis has been performed using the same database without considering historical data in order to realise the influence of the historical data in the regional analysis. A comparison between the results obtained through the FAB method performed for the skew surge database with and without historical data is displayed.

In the case in which a database is composed by only systematic data, the regional duration is considered effective like for the RFA approach.

Using only systematic skew surges, the performance of weighting analysis to compute the optimal value of $\lambda$ has to be repeated. In fact, the optimal $\lambda$ can be identified as an another $\lambda$ value between all the 176 $\lambda$-cases when a different database is used to generate the regional extreme data sample.

This frequentist analysis is performed for the Region 1 and the Region 2 as in the previous case. The optimal value of $\lambda$ is 0.84 for the Region 1 (the same $\lambda$ value identified through the weighting analysis for a database with historical data) and 1.7 for Region 2.

Frequentist regional estimations are computed for Region 1 and the Region 2 and they are shown in Tab. 8 and Tab. 9.

Regional return levels associated to a return period of 1000 years and their upper bounds of 90% confidence intervals are shown in Tab. 10 and Tab. 11 for the Region 1 and the Region 2. In addition, the relative widths of 90% confidence intervals are computed.

Regional return level plots for the Region 1 and the Region 2 are illustrated in Fig. 31 and Fig. 32.

| **Regional parameters of the Region 1 (without the use of historical data)** | | | | |
|---|---|---|---|---|
| *Optimal λ* | *Scale param. of regional GPD (season DJF)* | *Shape parameter of regional GPD* | *Regional effective duration (years)* | *Adimensional degree of regional dependence* |
| **0.84** | **0.199** | **0.052** | **514.28** | **0.543** |

*Tab. 8 - Regional parameters computed by the FAB method applied to the Region 1 without historical data*

| **Regional parameters of the Region 2 (without the use of historical data)** | | | | |
|---|---|---|---|---|
| *Optimal λ* | *Scale param. of regional GPD (season DJF)* | *Shape parameter of regional GPD* | *Regional effective duration (years)* | *Adimensional degree of regional dependence* |
| **1.7** | **0.243** | **0.036** | **235.88** | **0.677** |

*Tab. 9 - Regional parameters computed by the FAB method applied to the Region 2 without historical data*

Results of Tab. 8 and Tab. 9 are compared with these obtained by the use of historical data in the regional analysis in Tab. 3 and Tab. 5.

The application of FAB method with historical skew surges enables the estimation of a higher regional GPD shape parameter and of a bit higher regional duration for the Region 1. Other values figured out in Tab. 8 and in Tab. 3 are very close.

Also for the Region 2, the regional GPD shape parameter and the regional duration decrease without the use of historical data.

Results for these regions point out a common rise of the GPD scale parameter using historical data. In addition, a little growth of the period of observed regional extreme events has to be identified when historical data are used.

| **Results for the Region 1 (without the use of historical data)** | | |
|---|---|---|
| *Regional quantiles for T=1000ys* | *Regional upper CI 90% for T=1000ys* | *ΔCI90 / yR,T=1000ys (%)* |
| **2.55** | **2.90** | **28** |

*Tab. 10 - Regional return levels computed by the FAB method applied to the Region 1 without historical data*

| **Results for the Region 2 (without the use of historical data)** | | |
|---|---|---|
| *Regional quantiles for T=1000ys* | *Regional upper CI 90% for T=1000ys* | *ΔCI90 / yR,T=1000ys (%)* |
| **2.94** | **3.45** | **34** |

*Tab. 11 - Regional return levels computed by the FAB method applied to the Region 2 without historical data*

Results of Tab. 10 and Tab. 11 are compared with these obtained in Tab. 4 and Tab. 6.

For both the regions, the introduction of the extraordinary historical events tends to increase the value of return levels. In addition, the relative width of the confidence intervals is a bit lower (5-6 %) when historical data are not used. This trend is due to the exceptionality of the extreme

past events. In fact, the higher skew surges of the both regional extreme data samples are historical data. In any case, this value is acceptable for a statistical analysis.

Moreover, the use of historical data has increased the regional durations of the both regional extreme data samples. In particular, historical data allows the detection of three additional storms in the Region 1 and of five additional storms in the Region 2. In addition, other historical data are the biggest normalised data of five storms detected in the Region 1.

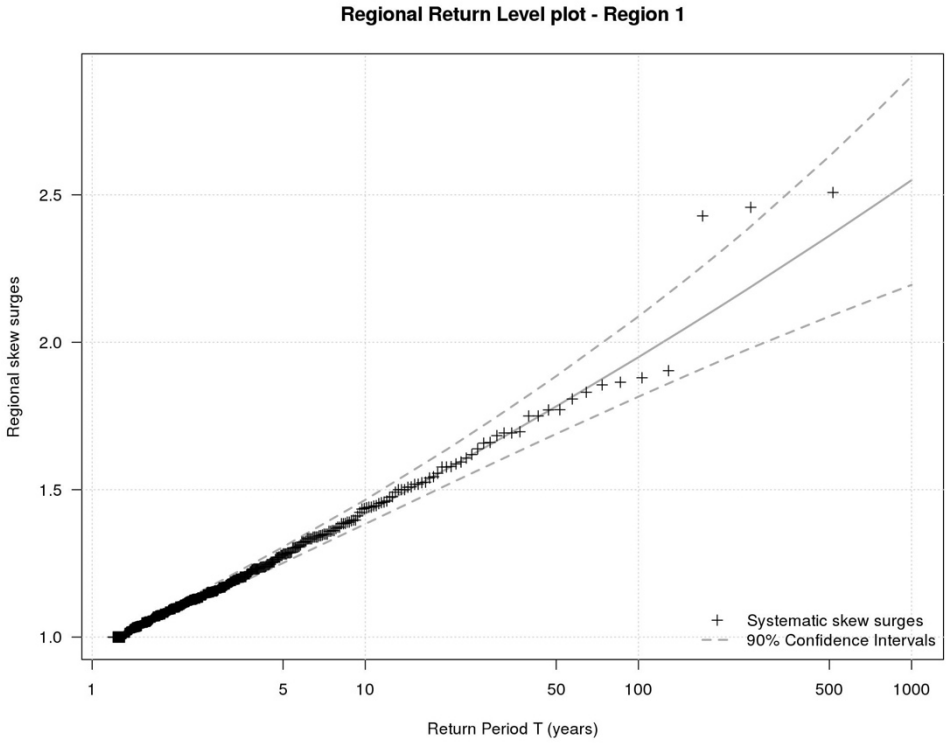


*Fig. 31 – Regional return level plot for the Region 1 without the use of historical data*

Fig. 31 shows graphically the decrease of high return levels when historical data are not considered in the statistical analysis.

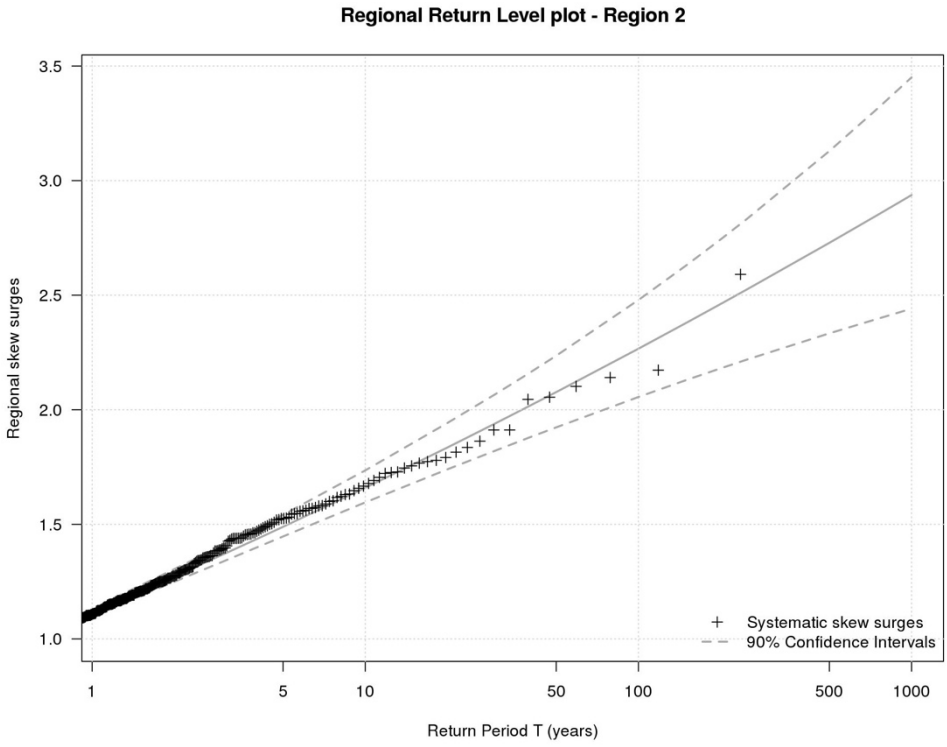


*Fig. 32 – Regional return level plot for the Region 2 without the use of historical data*

Fig. 32 illustrates the return level plot of the Region 2 without the five historical data used in the previous analysis.

However, regional return levels are normalised values and, for this reason, it is appropriate to compare also local return levels in order to provide global conclusions on this analysis of comparison.

Results at La Rochelle and at Calais are shown in Tab. 12 and Fig. 33 and they are compared respectively with Tab. 7 and Fig. 30. Same considerations on return levels can be pointed out for the local cases. In fact, return levels linked to a $T$ of 1000 years for the two sites of La Rochelle and Calais are lower than these obtained with historical data. The difference for these estimations is of 21 centimetres for the site of La Rochelle and of 16 centimetres for the site of Calais.

| La Rochelle | | | Calais | | |
|---|---|---|---|---|---|
| *Quantiles for T=1000ys (meters)* | *Upper CI 90% for T=1000ys (meters)* | *ΔCI90 / xT=1000ys (%)* | *Quantiles for T=1000ys (meters)* | *Upper CI 90% for T=1000ys (meters)* | *ΔCI90 / xT=1000ys (%)* |
| **1.61** | **1.84** | **29** | **1.62** | **1.90** | **35** |

*Tab. 12 - Results for the sites of La Rochelle (Region 1) and Calais (Region 2) without historical data*

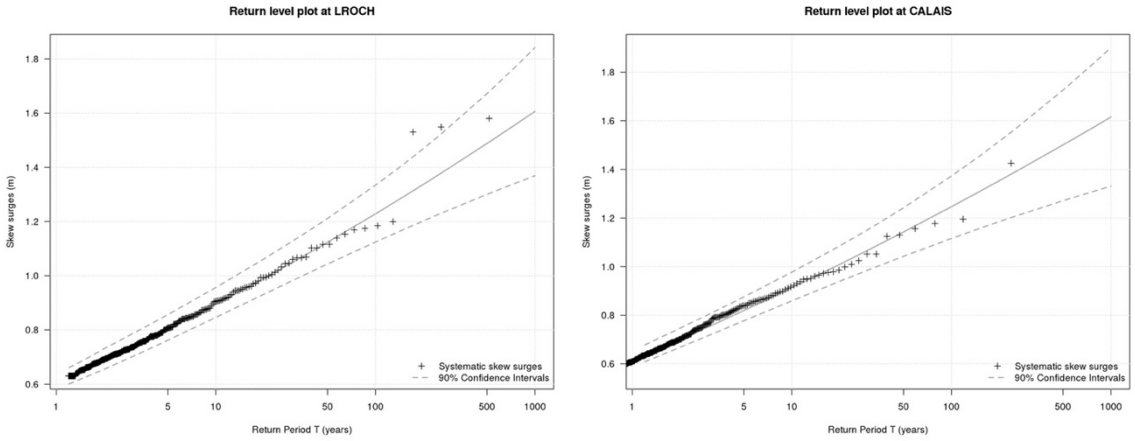


*Fig. 33 – Local return level plots for the sites of La Rochelle (on the left) and Calais (on the right) without the use of historical data*

In conclusion, for this particular application, historical data does not reduce the uncertainties on estimations of regional and local extreme events. This reduction could be obtained with the use of a big number of historical events.

On the contrary, the consideration of the extraordinary historical events has permitted the extension of the period of observation of the regional extreme data sample and the computation of more reliable extreme events. In particular, additional exceptional storms are detected and they have been used to perform this statistical analysis.

# 4.8 Bayesian estimations of return levels

Bayesian estimations of regional and local return levels associated to several return periods $T$ are computed through the application of the FAB method. In particular, Region 1 and Region 2 are analysed in the following. Predictive return levels $y^*_R$, standard estimative return levels $y_R$ and their Credibility Intervals are estimated and figured out in a same return level plot.

In any case, the Bayesian statistical framework requires the definition of a posterior distribution of the vector of parameters of the statistical distribution considered in order to estimate return levels.

In this analysis, the posterior distribution of the regional GPD parameters' vector $\theta$ is computed through the generation of three chains of one million of iterations $U$. The convergence of the MCMC process for these vectors $\theta$ must be achieved in every chain and between all the chains. The Gelman and Rubin test (Gelman and Rubin, 1992) is performed to test this convergence. This test allows the computation of a degree of convergence called Potential Scale Reduction Factor. A value close to 1 for the PSRF has to be computed in order to verify the convergence (it is suggested to get at least a PSFR smaller than 1.05).

The PSRF is estimate for a total of one million of iterations. Fig. 34 shows how this factor assumes a value very close to 1 for each regional GPD parameter of the Region 1 and Region 2.

In addition, the convergence is also verified by the test of Brooks (Brooks and Gelman, 1998). This test is an implementation of Gelman and Rubin test and allows the estimation of another degree of convergence called Multivariate PSFR. This factor considers the likely variability that the sample could have.

The MPSFR must assume lower values than 1.2 to verify the convergence of MCMC iterations. MPSFR is considerably smaller than 1.2 for the Region 1 and the Region 2.

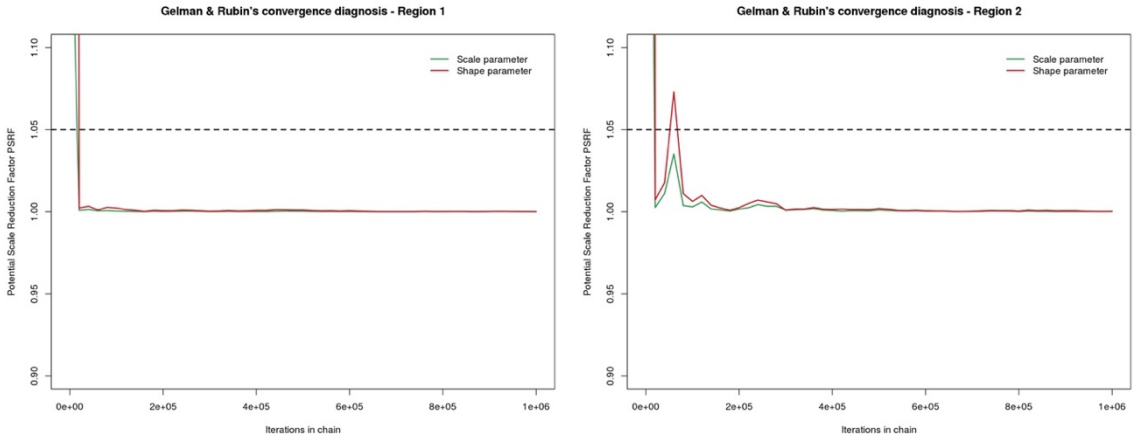


*Fig. 34 – Progressive PSFR values of tests of Gelman and Rubin for Region 1 and Region 2*

Values of the scale and the shape parameters obtained for every MCMC iteration and for each chain is shown in Fig. 35 and Fig. 36.

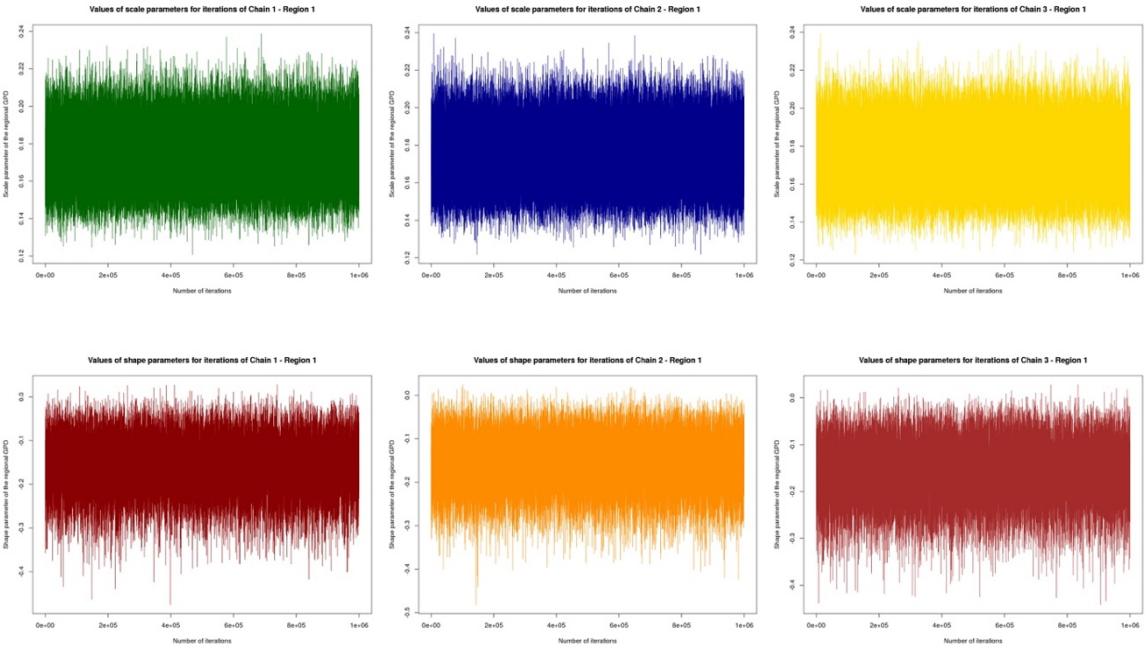


*Fig. 35 – Values of regional GPD scale and shape parameters of each iteration for the 3 chains of Region 1*

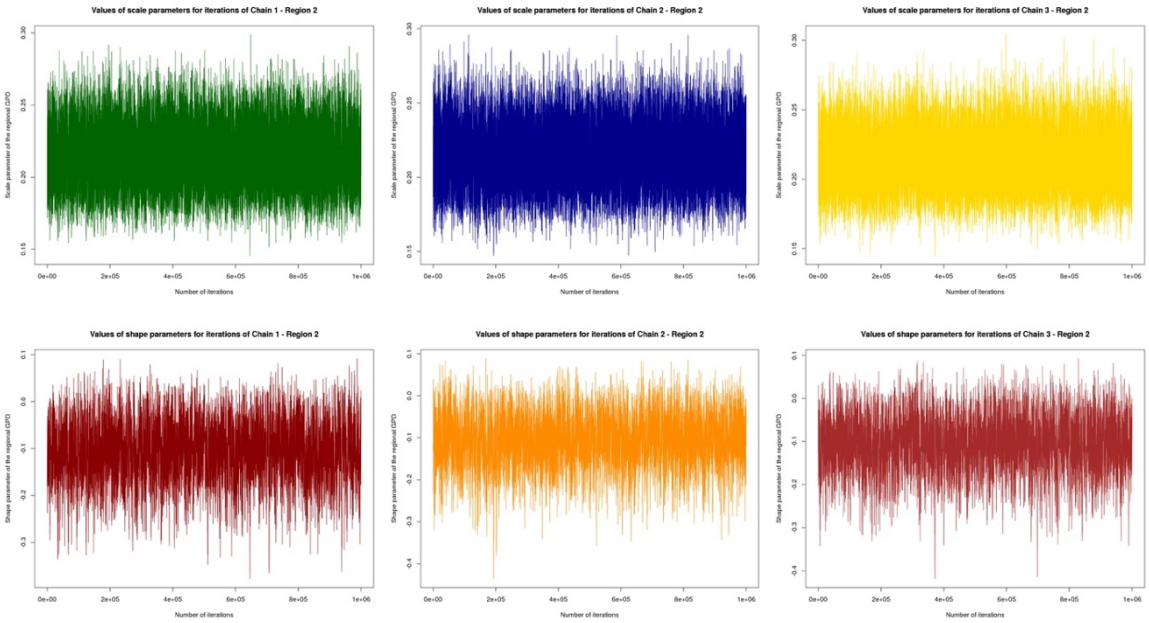


*Fig. 36 - Values of regional GPD scale and shape parameters of each iteration for the 3 chains of Region 2*

The verification of the convergence of the MCMC process enables the use of the posterior distribution of the regional GPD parameters' vector $\theta$ in the Bayesian estimation process of return levels.

The Bayesian estimation of regional return levels can be now performed for the Region 1 and the Region 2. The results of this statistical analysis are are shown in Tab. 13 and Tab. 14. In particular, the predictive return levels are computed after a burn-in of $U'=10^5$ iterations.

| **Parameters and results for the Region 1** | | | | | | |
|---|---|---|---|---|---|---|
| *Optimal λ* | *Scale param. of estimative regional GPD* | *Shape param. of estimative regional GPD* | *Regional estimative quantiles for T=1000ys* | *Regional predictive for T=1000ys* | *Regional upper CI 90% for T=1000ys* | *ΔCI90 / yR,T=1000ys (%)* |
| **0.84** | **0.175** | **0.144** | **2.99** | **3.14** | **3.91** | **44** |

*Tab. 13 - Useful parameters and results computed by the Bayesian analysis on the Region 1*

| Parameters and results for the Region 2 | | | | | | |
|---|---|---|---|---|---|---|
| *Optimal λ* | *Scale param. of estimative regional GPD* | *Shape param. of estimative regional GPD* | *Regional estimative quantiles for T=1000ys* | *Regional predictive for T=1000ys* | *Regional upper CI 90% for T=1000ys* | *ΔCI90 / yR,T=1000ys (%)* |
| **1.79** | **0.216** | **0.089** | **3.30** | **3.51** | **4.56** | **53** |

*Tab. 14 - Useful parameters and results computed by the Bayesian analysis on the Region 2*

Tab. 13 and Tab. 14 display the regional results of the Bayesian analysis performed through the FAB method. Regional factors as the regional credible duration or the adimensional degree of regional dependence $\Phi$ are not figured because they are identic to that shown in Tab. 3 and Tab. 5. In fact, the Bayesian framework of estimation does not modify the computation of the main elements of the regional analysis. On the contrary, estimations of the statistical distribution's parameters and return levels can assume different values.

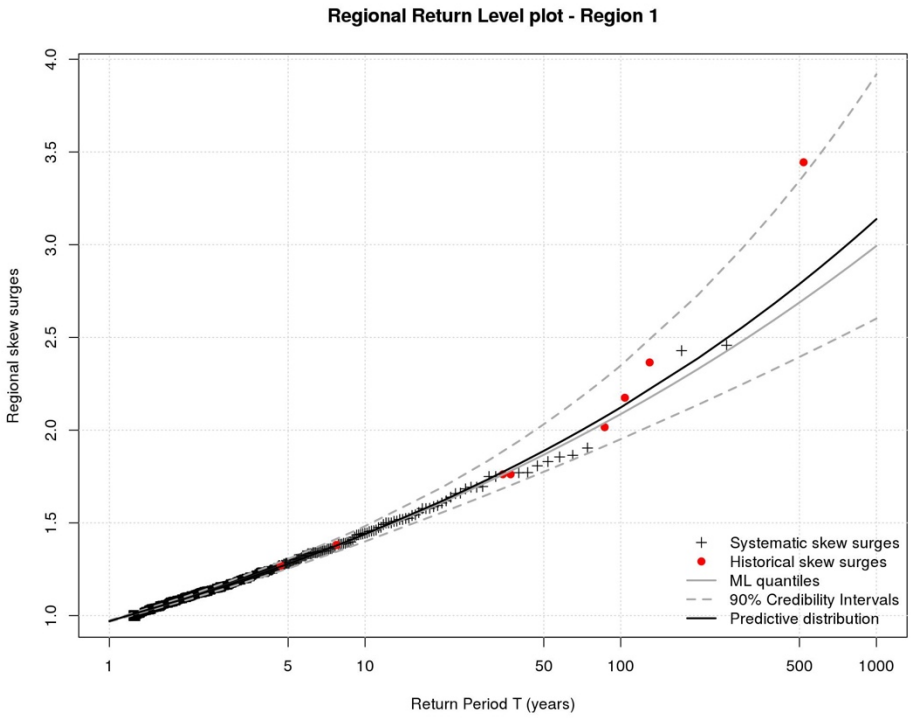


*Fig. 37 – Regional return level plot of Bayesian estimations for Region 1*

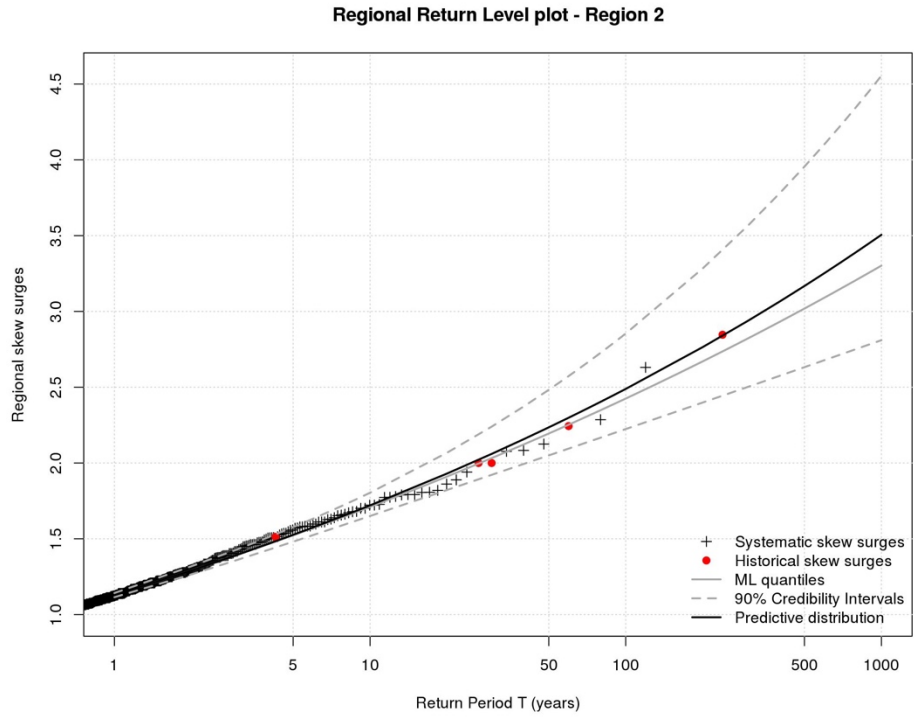


*Fig. 38 - Regional return level plot of Bayesian estimations for Region 2*

Fig. 37 and Fig. 38 display return level plots of Region 1 and Region 2. They highlight how the predictive return levels (in black) linked to a generic return period *T* are bigger than the estimative return levels (in grey) associated to the same generic return period *T*. In addition, Credibility Intervals are illustrated by the grey dotted lines. In these figures, historical data are represented as red dots in order to point out their relevance compared with the systematic events. All the empirical events are located in the return level plot by a Weibull position (Weibull, 1951).

However, these results can be locally evaluated in order to know the effective impact of these estimations. Local return levels are then computed from regional return levels by the use of local indexes. Same sites of the frequentist analysis are considered: La Rochelle for the Region 1 and Calais for the Region 2.

| La Rochelle | | | Calais | | |
|---|---|---|---|---|---|
| *Estimative quantiles for T=1000ys (meters)* | *Predictive quantiles for T=1000ys (meters)* | *Upper CI 90% for T=1000ys (meters)* | *Estimative quantiles for T=1000ys (meters)* | *Predictive quantiles for T=1000ys (meters)* | *Upper CI 90% for T=1000ys (meters)* |
| **1.88** | **1.97** | **2.47** | **1.78** | **1.89** | **2.46** |

*Tab. 15 – Bayesian estimations for the sites of La Rochelle (Region 1) and Calais (Region 2)*

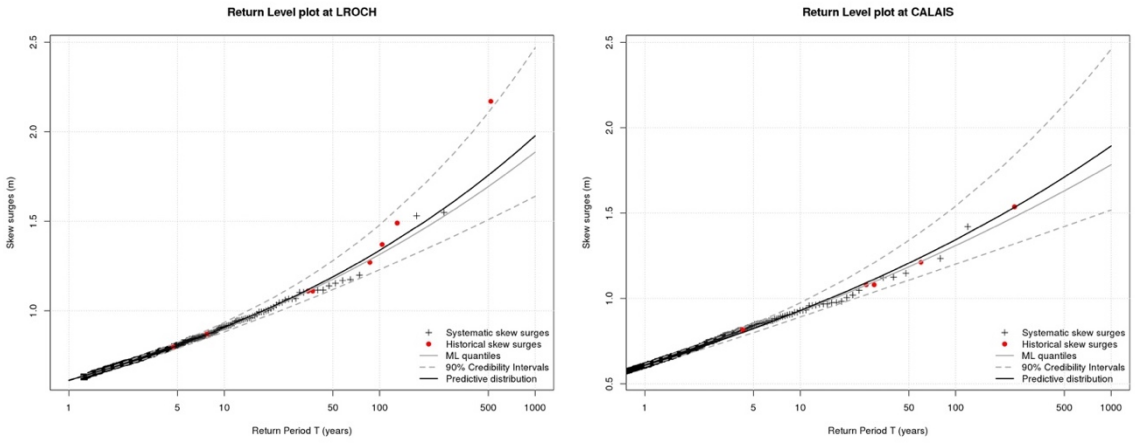


*Fig. 39 - Return level plots of Bayesian estimations for La Rochelle (site belonging to Region 1) and Calais (site belonging to Region 2)*

Same conclusions supplied for the regional Bayesian estimations can be provided for the local Bayesian estimations. Predictive return levels linked to a particular return period *T* are higher than standard estimative return levels estimated for the same particular return period.

Further clarifications have to be provided for the computation of the relative width of the Credibility Intervals. Regional and local CI have the same relative width in this analysis. In fact, the computation of regional and local CI considers in a Bayesian application of the FAB method only the variation of the return levels and not of the local indexes (as performed in frequentist by the bootstrap methodology).

# 4.9 Frequentist and Bayesian estimations

The comparison of the results of the frequentist and Bayesian statistical frameworks is not totally correct due to two different concepts of probability. Nevertheless, a preliminary comparison is performed in order to realise the differences obtained computing frequentist and Bayesian estimations with the FAB method.

In the Bayesian context, FAB method is performed considering the seasonal effects of the skew surges in the estimation process of the regional GPD parameters. For this reason, a particular case of frequentist estimations that not consider the seasonality of the skew surges has to be achieved. This case enables the preliminary comparison of these two statistical frameworks of estimation.

The value of optimal $\lambda$ is the same for Region 1 and for Region 2 (respectively 0.84 and 1.79) for this frequentist case. Results and regional return levels are displayed in Tab. 16 and Fig. 40.

The comparison between the 90% Confidence Intervals of Tab. 16 with the previous 90% Credibility Intervals computed in the previous Bayesian analysis has to be carefully performed. In fact, in the frequentist framework the Confidence Intervals are calculated through a bootstrap method while in the Bayesian framework the Credibility Intervals are computed by the definition of the posterior distribution.

| **Frequentist estimations for the Region 1 and Region 2** | | | | | |
|---|---|---|---|---|---|
| **Region 1** | | | **Region 2** | | |
| *Optimal* $\lambda$ | *Regional upper CI 90% for T=1000ys* | *ΔCI90 / yR,T=1000ys (%)* | *Optimal* $\lambda$ | *Regional upper CI 90% for T=1000ys* | *ΔCI90 / yR,T=1000ys (%)* |
| **0.84** | **3.59** | **37** | **1.79** | **4.01** | **40** |

*Tab. 16 - Useful parameters and results computed by the Bayesian analysis on the Region 1 without seasonality*

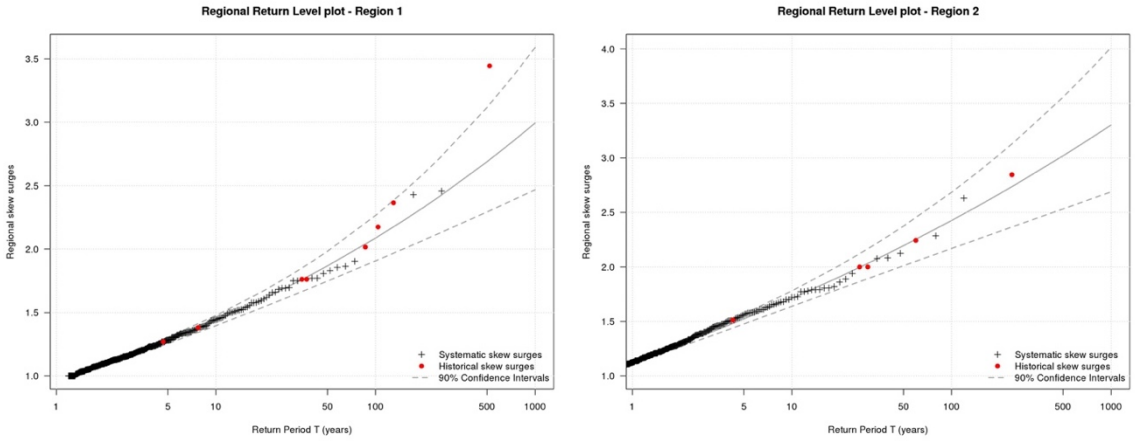


*Fig. 40 – Regional return level plot of frequentist estimations for Region1 and Region 2 without seasonality*

Comparing regional results obtained in Tab. 16 and those illustrated in Tab. 13 and Tab. 14, Credibility Intervals tend to be more unbounded than Confidence Intervals in this application. This is pointed out by the relative widths of the Credibility Intervals that assume higher values of percentage for a return period *T* of 1000 years compared with Confidence Intervals linked to the same return period *T*.

Same considerations can be provided for the local estimations of Tab. 17 and Fig. 41 compared with Bayesian local estimations of Tab. 15 and Fig. 39.

| **La Rochelle** | | **Calais** | |
|---|---|---|---|
| *Upper CI 90% for T=1000ys (meters)* | *ΔCI90 / yR,T=1000ys (%)* | *Upper CI 90% for T=1000ys (meters)* | *ΔCI90 / yR,T=1000ys (%)* |
| **2.28** | **39** | **2.15** | **40** |

*Tab. 17 - Frequentist estimations for the sites of La Rochelle (Region 1) and Calais (Region 2) without seasonality*

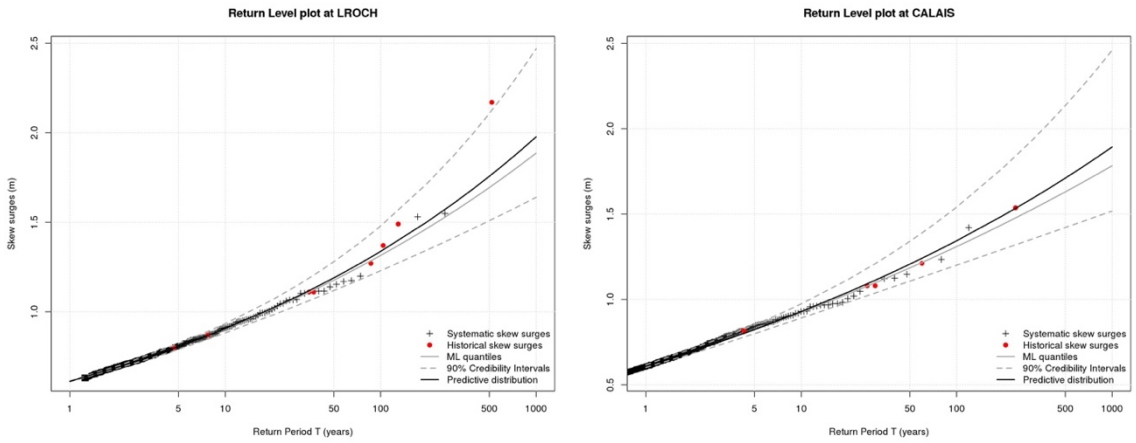


*Fig. 41 - Return level plots of frequentist estimations for La Rochelle (site belonging to Region 1) and Calais (site belonging to Region 2) without seasonality*

As for Bayesian estimations, results and local return levels are figured out for the site of La Rochelle (Region 1) and for the site of Calais (Region 2).

Significant differences are identified between the upper 90% Confidence Interval for a return period T of 1000 years computed by this particular frequentist analysis (Tab. 17) and the upper 90% Credibility Interval for the same return period *T* (Tab. 15). For the site of La Rochelle, this difference is of 18 centimetres and for Calais is of 30 centimetres.

Finally, for this case of study, Bayesian estimations obtained by the application of the FAB method provide higher uncertainties linked to very high return period *T* than the frequentist estimations linked to the same return period *T*. On the other hand, the use of the Bayesian framework allows the utilisation of a prior information that the expert could know and the computation of the predictive distribution of the extreme data sample.

All frequentist and Bayesian estimations of this study obtained with and without the use of historical data are synthetized in the summary table displayed in the Annexe E.